Thallium isotopic composition of phlogopite in kimberlite-hosted MARID and PIC mantle xenoliths

Angus Fitzpayne [1,2]*, Julie Prytulak [3,4], Andrea Giuliani [1,2], Janet Hergt [1]

* *Corresponding author; email: afitzpayne@ethz.ch*

(ORCiD: 0000-0002-6020-0341)

[1] *KiDs (Kimberlites and Diamonds) Research Group, School of Earth Sciences, The University of Melbourne, Parkville 3010, Victoria, Australia*

[2] *Institute of Geochemistry and Petrology, Department of Earth Sciences, ETH, Clausiusstrasse 25, CH-8092 Zurich, Switzerland*

[3] *Department of Earth Science and Engineering, Imperial College London, Exhibition Road, London SW7 2AZ, United Kingdom*

[4] *Department of Earth Science, University of Durham, DH1 3LE, United Kingdom*

Abstract: 405 words

Text + figure captions: 8578 + 977 words

9 figures

2 tables

108 references

Keywords: *MARID; mantle metasomatism; thallium; isotope geochemistry*

Abstract

MARID (Mica-Amphibole-Rutile-Ilmenite-Diopside) and PIC (Phlogopite-Ilmenite-Clinopyroxene) rocks are rare mantle xenoliths entrained by kimberlites. Their high phlogopite modes (15 to ~100 vol.%) and consequent enrichments in alkali metals and H_2O suggest a metasomatic origin. Phlogopite also has high concentrations (>0.2 μg/g) of thallium (Tl) relative to mantle abundances (<3 ng/g). Thallium isotope ratios have proven useful in tracing the input of Tl-rich materials, such as pelagic sediments and altered oceanic crust, to mantle sources because of their distinct isotopic compositions compared to the peridotitic mantle. This study presents the first Tl isotopic compositions of well-characterised phlogopite separates from MARID and PIC samples to further our understanding of their genesis. The PIC rocks in this study were previously interpreted as the products of kimberlite melt metasomatism, whereas the radiogenic and stable N-O isotope systematics of MARID rocks suggest a parental metasomatic agent containing a recycled component.

The ε^{205}Tl values of phlogopite in both PIC (–2.7 ± 0.8; 2 s.d., n = 4) and MARID samples (–2.5 ± 1.3; 2 s.d., n = 21) overlap with the estimated mantle composition (–2.0 ± 1.0). PIC phlogopite Tl contents (~0.4 μg/g) are suggestive of equilibrium with kimberlite melts (0.1–0.6 μg/g Tl), based on partitioning experiments in other silica-undersaturated melts. Kimberlite Tl-ε^{205}Tl systematics suggest their genesis does not require a recycled contribution: however, high temperature-altered oceanic crust cannot be ruled out as a component of the Kimberley kimberlites' source.

Mantle-like ε^{205}Tl values in MARID samples also seem to contradict previous suggestions of a recycled contribution towards their genesis. Recycled components with isotopic compositions close to mantle values (e.g., high temperature-altered oceanic crust) are still permitted. Moreover, mass balance mixing models indicate that incorporation into the primitive mantle of 1–30% of a low temperature-altered oceanic crust + continental crust recycled component or 1–50% of continental crust alone could be accommodated by the Tl–ε^{205}Tl systematics of the MARID parental melt. This scenario is consistent with experimental evidence and existing isotopic data. One PIC phlogopite separate has an extremely light Tl isotopic composition of –9.9, interpreted to result from kinetic isotopic fractionation. Overall, phlogopite is the main host mineral for Tl in metasomatised mantle and shows a very restricted range in Tl isotopic composition, which overlaps with estimates of the mantle composition. These results strongly suggest that negligible high temperature equilibrium Tl isotopic fractionation occurs during metasomatism and reinforces previous estimates of the mantle's Tl isotopic composition.

1 Introduction

The subcontinental lithospheric mantle (SCLM) is heterogeneous, both mineralogically and chemically (e.g., Erlank et al., 1987; Jones et al., 1982). The SCLM beneath the Kaapvaal craton in southern Africa is thought to be the residue of high degree partial melting (>50%), based on mineral inclusions with refractory compositions preserved in diamonds (e.g., Banas et al., 2009; Phillips et al., 2004) as well as experimental studies of partial melting of fertile peridotites at high pressure and temperature (Herzberg,

2004; Walter, 1998). However, it is evident that several metasomatic events have since affected the Kaapvaal SCLM and introduced volatile-rich and/or exotic phases including phlogopite, K-richterite, and titanates (e.g., Aoki, 1974; Erlank and Finger, 1970; Haggerty, 1983). Many studies have also reported the occurrence of phlogopite-rich (and olivine-free), ultramafic mantle rocks (previously "glimmerites") amongst kimberlite xenolith suites, and particularly those from South African localities (e.g., Dawson and Smith, 1977; Grégoire et al., 2002; Waters 1987), although they do occur elsewhere (e.g., Canada; Peterson and le Cheminant, 1993). Such phlogopite-rich lithologies have often been cited as important source components from which alkaline magmas are derived (e.g., Foley, 1992). Many early studies attributed phlogopite-rich metasomatism to interactions with kimberlite melts (Dawson and Smith, 1977; Gurney and Harte, 1980; Harte et al., 1993). More recently, geochemical and isotopic compositions have been used to divide phlogopite-rich rocks into two groups named MARID (Mica-Amphibole-Rutile-Ilmenite-Diopside) and PIC (Phlogopite-Ilmenite-Clinopyroxene: e.g., Fitzpayne et al., 2018a; Grégoire et al., 2002, and references therein). Both lithologies are derived from the lithospheric mantle, and are transported to the Earth's surface primarily by kimberlites; however, radiogenic isotope and trace element data suggest that the genesis of only the PIC suite – and related rocks, for example some lherzolites (cf. Bussweiler et al., 2018) and wehrlites (Fitzpayne et al., *in press*) – can be closely related to kimberlite melt metasomatism (Fitzpayne et al., 2018a, 2019). In contrast, MARID rocks may be related to interactions between the mantle and orangeite/lamproite melts (e.g., Hamilton et al., 1998; Konzett et al., 1998) or other alkaline, mafic magmas (e.g., relating to the Karoo large igneous province: Giuliani et al., 2014a; Konzett et al., 1998; van Achterbergh et al, 2001). Several investigations of MARID rocks have suggested that their source rocks likely require a

recycled component (e.g., Fitzpayne et al., 2019, *in press*). Uncertainties remain regarding the identity of this recycled component, which might be resolved by employing alternative isotope systems to those studied to date (N, O, Sr, Nd, Hf, Pb). The thallium (Tl) isotope system has been successfully used to trace the contributions of recycled material (altered oceanic crust, sediments) to subduction-related magmas (e.g., Nielsen et al., 2016, 2017b; Prytulak et al., 2013; Shu et al., 2017). Moreover, micas are likely the main hosts for Tl in most igneous rocks (e.g., Rader et al., 2018). Here, we present the first investigation of the Tl isotopic composition of mica separates from mantle-derived MARID and PIC rocks to provide new information about the sources of phlogopite-rich metasomatism and its implications towards subduction and the evolution of the mantle.

1.1 MARID and PIC rocks

MARID and PIC rocks are coarse-grained, ultrapotassic and ultramafic rocks (e.g., Dawson and Smith, 1977; Waters, 1987) that are most commonly found as xenoliths entrained by the Kimberley kimberlites in South Africa (e.g., Grégoire et al., 2002). MARID and PIC rocks are predominantly composed of phlogopite, which results in large ion lithophile element (LILE) enrichment (4–10 wt.% K_2O; Grégoire et al., 2002; Waters, 1987), relative to the primitive mantle (McDonough and Sun, 1995). No geochronological or thermobarometric work has been undertaken on PIC samples due to the lack of mineral assemblages upon which such studies can be conducted. Despite this, a genetic link between kimberlites and PIC samples has been well established, based on trace element compositions and overlapping radiogenic isotopic compositions (Fitzpayne et al., 2018a, 2019; Grégoire et al., 2002). It appears unlikely that PIC rocks are the source of kimberlite magmatism, because they display petrographic evidence of

kimberlite melt infiltration — such as inclusions of kimberlite magmatic minerals (e.g., calcite, apatite, perovskite) in reacted PIC clinopyroxene rims (Fitzpayne et al., 2018b). Kimberlite melt infiltration likely occurred shortly before or during entrainment in the host kimberlite magma, based on the preservation of disequilibrium features such as clinopyroxene zonation. PIC rocks have therefore been inferred to be the metasomatic products of failed kimberlite intrusions, which reacted with peridotite protoliths (Fitzpayne et al., 2018a, b).

Geochronological constraints for MARID samples provide minimum crystallisation ages of between 130–140 Ma (zircon U-Pb; Giuliani et al., 2015; Konzett et al., 1998) and 170 Ma (bulk-rock Re-Os; Pearson et al., 1995), which have led to suggestions by the same authors of a genetic link to Karoo magmatism. MARID rocks likely reside within the lithospheric mantle, based on limited thermobarometric data (4.2 GPa, 960 °C from Ca-in-orthopyroxene thermobarometry: Konzett et al., 2014), as well as experimental evidence that phlogopite and K-richterite can be stable to pressures of up to 8.5 GPa (i.e., at or below the lithosphere-asthenosphere boundary beneath the Kaapvaal craton; e.g., Konzett et al., 1997). There is also natural evidence (mineral inclusions in diamonds) that MARID rocks may occur within the diamond stability field (Meyer and McCallum, 1986), which for the Kaapvaal craton is equivalent to pressures > ~4.5 GPa (i.e. depths of ~ 150 km; e.g., Kennedy and Kennedy, 1976; Mather et al., 2011; O'Reilly and Griffin, 2006).

Radiogenic isotope data for MARID minerals (clinopyroxene and amphibole) suggest that MARID rocks have "enriched mantle" signatures (e.g., $^{87}Sr/^{86}Sr_i$ ~ 0.711; Fitzpayne et al., 2019) prior to kimberlite entrainment and infiltration. Such compositions may be related to a contribution from recycled crustal components, prolonged storage of incompatible element-enriched material in the lithospheric mantle,

or a combination thereof. Several investigations have found trace element similarities in clinopyroxene in MARID and lherzolite samples derived from southern African and other kimberlites (e.g., Aulbach et al., 2013; Grégoire et al., 2003; Rehfeldt et al., 2008). This inference has recently been extended to other geochemical and stable isotope systematics (Fitzpayne et al., *in press*), which indicate that the genesis of MARID and some lherzolites can be related to a similar metasomatic fluid. The presence of a recycled component in both MARID rocks and some lherzolites is further supported by high $\delta^{15}N$ (up to +9 ‰: Banerjee et al., 2015) and low $\delta^{18}O$ values (as low as +4.4 ‰: Fitzpayne et al., *in press*) in phlogopite and clinopyroxene, respectively, relative to reported values for the ambient mantle ($\delta^{15}N = -5 \pm 2$ ‰: Marty and Dauphas, 2003; $\delta^{18}O_{cpx} = +5.5 \pm 0.7$ ‰: Mattey et al., 1994). Low $\delta^{18}O$ values from MARID and related lherzolite samples from Kimberley suggest that the parental metasomatic fluid incorporated a high temperature-altered oceanic crust component. However, low $\delta^{34}S$ values in sulfides from the same lherzolites (–5.9 to –2.1 ‰: Giuliani et al., 2016) are more likely to relate to incorporation of sedimentary sulfides (e.g., Farquhar et al., 2010) or low temperature-altered oceanic crust (Alt and Shanks, 2011). Based on these data, the nature of recycled components in the source of the MARID metasomatic agent(s) remains uncertain. This contribution combines previously reported petrographic, geochemical, and isotopic data for MARID and PIC rocks with new mica Tl isotopic compositions, in order to further our understanding of the causes and sources of phlogopite-rich metasomatism in the SCLM.

1.2 Geochemistry and isotope systematics of thallium

Thallium is a volatile and highly incompatible trace metal with two redox states (Tl^+ and Tl^{3+}). In igneous systems, Tl only exists as Tl^+ (e.g., Nielsen et al., 2017a), whereas

the Tl^{3+} species occurs in oxidising conditions at the surface of the Earth (Batley and Florence, 1975; Vink, 1993). Due to its large ionic radius (Tl^{+}: 1.49 Å; Shaw, 1952), Tl behaves similarly to the LILE (especially K^{+}: 1.33 Å; Rb^{+}: 1.49 Å; Cs^{+}: 1.65 Å; e.g., Shaw, 1952) and is incompatible during mantle partial melting. Consequently, Tl is more abundant in the continental crust (0.5–1.6 µg/g; Rudnick and Gao, 2014) compared to the primitive mantle (~0.0035 µg/g; McDonough and Sun, 1995). The similarity between alkali metals and Tl also extends to their tendency to be fluid-mobile (e.g., Vink, 1993). Experimental investigations have shown that Tl is compatible in K-rich phases such as biotite (e.g., $^{\text{biotite-melt}}D_{Tl}$ = 8.6; Bea et al., 1994). Mica (biotite, muscovite, and phlogopite) and other phyllosilicate (chlorite) mineral separates (n = 45) from a variety of crustal igneous, metamorphic, and metasomatic environments have Tl abundances between 0.2 and 22.5 µg/g (Rader et al., 2018), with most having greater concentrations than continental crust estimates (Fig. 1).

Thallium can also display strong affinities to sulfur-rich phases (McGoldrick et al., 1979; Noll et al., 1996). Some experimental studies have suggested that Tl preferentially partitions into sulfide liquids in equilibrium with basaltic melts (at 1400 °C and 1.5 GPa: e.g., Kiseeva and Wood, 2013). However, the majority (24 out of 38) of natural sulfide samples contain undetectable amounts of Tl (<0.2 µg/g; Rader et al., 2018), or more generally contain lower Tl than phlogopite (Fig. 1).

Thallium has two stable isotopes, ^{203}Tl (29.5%) and ^{205}Tl (70.5%), ratios of which are reported in parts per ten thousand (ε units) relative to the NIST Tl reference material SRM997, which is defined as 0, where

$$\varepsilon^{205}\text{Tl} = 10^4 \text{ x } \frac{^{205}\text{Tl}/^{203}\text{Tl}_{\text{sample}} - {}^{205}\text{Tl}/^{203}\text{Tl}_{\text{SRM997}}}{^{205}\text{Tl}/^{203}\text{Tl}_{\text{SRM997}}}$$

Thallium isotopes have been used for a variety of applications (Nielsen et al., 2017a, and references therein), including the characterisation of terrestrial Tl cycling between the crust and the mantle via subduction zones. It might first seem that Tl would be unable to contribute to these studies, as the Tl isotopic composition of the bulk continental crust (based on loess samples: $\varepsilon^{205}Tl = -2.0 \pm 0.5$; 2 s.d.; Nielsen et al., 2005) is identical to the reported mantle value ($\varepsilon^{205}Tl = -2.0 \pm 1.0$; 2 s.d.), based on the analysis of MORB glass samples from various ocean basins (Nielsen et al., 2006a, 2017a). Furthermore, it has been suggested that magmatic processes, including melting and fractional crystallisation of anhydrous lavas, do not cause analytically resolvable differences in $\varepsilon^{205}Tl$ (Hettmann et al., 2014; Prytulak et al., 2013, 2017). Although this implies that the $\varepsilon^{205}Tl$ value of subducted material should be reflected in any later-derived mantle metasomatic or melting products (e.g., arc lavas), this does not appear to be helpful if crustal and mantle lithologies display similar Tl isotopic ratios. However, rocks that have been altered in low temperature environments can display significant shifts in Tl isotopic composition. Oceanic ferromanganese sediments and pelagic clays preferentially incorporate ^{205}Tl ($\varepsilon^{205}Tl$ from +2 to +15; Rehkamper et al., 2002, 2004), whereas the lighter ^{203}Tl isotope becomes preferentially concentrated in low temperature hydrothermally-altered oceanic crust ($\varepsilon^{205}Tl$ as low as –16; Coggon et al., 2014; Nielsen et al., 2006a). Consequently, many studies have employed Tl isotopes as a tracer for recycled material, for example of Fe-Mn sediments in ocean island basalts (Nielsen et al., 2006b, 2007) or the relative contribution of pelagic clays and altered oceanic crust in island arc magmatism (Nielsen et al., 2016, 2017b; Prytulak et al., 2013; Shu et al., 2017). Mineral separates of clinopyroxene and garnet from six bulk-rock eclogite samples from the Kaalvallei (kimberlite) and Bellsbank (orangeite) localities in South Africa have also been characterised for their Tl isotopic compositions by Nielsen et al.

(2009). Only one recalculated bulk-rock sample (–5.1 ± 1.0) displays a negative excursion from the mantle ε^{205}Tl value, inferred to represent low temperature-altered oceanic crust that had been subducted and incorporated into the lithospheric mantle. In contrast, high temperature-altered oceanic basalts have ε^{205}Tl values (~ –2) and very low Tl concentrations (0.005 μg/g), similar to those of the mantle (e.g., Nielsen et al., 2006a). Shu et al. (2019) recently analysed ~60 bulk-rock eclogite samples from several localities worldwide, which displayed ε^{205}Tl values of between -5.6 and +0.7. This range was interpreted to reflect the differences in protolith as well as the metamorphic/metasomatic history in each locality.

Thallium isotopic variations in the reservoirs mentioned above have largely been interpreted to reflect equilibrium fractionation. However, Nielsen et al. (2017a) suggested that kinetic effects might be (partly) responsible for large isotopic excursions from the mantle value (of up to ~10 ε units) during hydrothermal alteration of oceanic crust. They also note that equilibrium isotopic effects might be responsible for large ε^{205}Tl shifts if the oxidised Tl^{3+} species were present. Such effects might be better characterised by conducting studies upon mineral separates and not bulk-rock samples, and emphasises the need to collect petrographic information to aid the interpretation of isotopic data.

2 Samples

The xenolith samples analysed in this study were collected from kimberlite (Bultfontein, De Beers, Kamfersdam, Kimberley, Wesselton) and orangeite (Newlands) localities in the Kimberley block of the Kaapvaal craton, South Africa (Fig. 2; Field et

al., 2008). The emplacement of the Kimberley kimberlites (~84 Ma: Kramers et al., 1983) occurred after the intrusion of orangeites at Newlands (114 ± 1 Ma: Smith et al., 1985).

All xenolith samples were selected from the collections housed in the John J. Gurney Upper Mantle Research Collection at the University of Cape Town and the De Beers Consolidated Mines rock store, or were collected during field work in the Boshof Road dumps, which comprise waste material from historical mining of the Bultfontein kimberlite. The samples investigated in this study display a variety of textures including granular, foliated, and porphyroclastic (Fig. 3; Table 1). The modal mineral abundances in MARID and PIC rocks are notoriously heterogeneous (Grégoire et al., 2002; Waters, 1987), and the samples in this study likewise have extremely variable amounts of phlogopite (20–100 vol.% and 80–100 vol.%, respectively: Fitzpayne et al., 2018a). Phlogopite is the dominant Tl host in MARID and PIC mantle xenoliths (e.g., MARID mica average = 2.1 ± 5.9 μg/g Tl; 2 s.d., n = 147: Fitzpayne et al., 2018a). MARID and PIC phlogopite core Tl contents vary between 0.3 and ~10 μg/g, and are always higher than those of coexisting minerals (K-richterite: <0.1 μg/g; clinopyroxene: <0.02 μg/g; ilmenite: <0.01 μg/g; rutile: <0.005 μg/g; Fitzpayne et al., 2018a, b). This observation is consistent with that of Rader et al. (2018), who also show that phlogopite from a variety of geological environments commonly has a much greater Tl content than its coexisting minerals. Although Tl concentration is not routinely analysed, there are a few studies that provide further evidence that common mantle minerals do not contain high Tl abundances. For example, an olivine/orthopyroxene/spinel-dominated harzburgite from the Eifel (Germany) volcanic field has a bulk-rock Tl content of 0.00105 μg/g (Klein et al., 2015), and peridotites from the Balmuccia Massif in Italy have Tl <0.00355 μg/g (n = 17; Wang et al., 2018).

Analysis of mineral separates may circumvent uncertainties regarding bulk-rock analyses of mantle samples as proxies for the mantle's Tl isotopic composition, which may be hampered by kimberlite (i.e. entraining magma) contamination (e.g., Nielsen et al., 2009) and the presence of interstitial sulfides (e.g., Nielsen et al., 2014). The latter issue may not be as significant as previously thought, since Tl partitioning into sulfide phases appears to be minor, particularly when phyllosilicates such as micas are also present (Fig. 1; Rader et al., 2018). Importantly, the Tl content in mica is also much greater than the abundance of Tl in the Kimberley kimberlites (bulk-rock: 0.25 ± 0.23 μg/g Tl; 1 s.d., n = 5: Muramatsu, 1983), which suggests that mica Tl isotopic compositions are unlikely to be affected by interstitial kimberlitic material.

Several different textural modes of phlogopite occur in the studied samples. In MARID rocks, phlogopite occurs both as a coarse-grained (typically >200 μm) "primary" matrix mineral (with variable amounts of zonation; Fig. 3a), and as a finer-grained (generally <50 μm) "secondary" phase in carbonate- or serpentine-rich pools or veins. Phlogopite rims and vein-hosted phlogopite have both been shown to be compositionally distinct from "primary" MARID groundmass phlogopite, and both features are likely related to infiltration of the xenoliths by the host kimberlite magma (Fitzpayne et al., 2018b). In contrast, PIC rocks typically contain unzoned, coarse-grained (>100 μm) phlogopite porphyroclasts that are surrounded by euhedral neoblasts of fine-grained phlogopite (<50 μm). Carbonates are commonly found interstitially between phlogopite grains in PIC rocks, and both their presence and the sheared textures in PIC rocks may be attributed to interactions with the entraining kimberlite melt (Fitzpayne et al., 2018b). There appear to be few differences between the major element compositions of PIC phlogopite porphyroclasts and neoblasts; however, only

porphyroclastic phlogopite was targeted for *in situ* LA-ICP-MS trace element analysis (Fitzpayne et al., 2018a, b).

3 Methods

Small rock chips of MARID and PIC samples were crushed using either a jaw crusher or a steel percussion mortar, before being sieved into several size fractions. Phlogopite grains were hand-picked under a binocular microscope, focussing on relatively coarse size fractions (125–500 μm) in order to select only monomineralic grains, as well as to minimise contamination from fine-grained vein-hosted or neoblastic phlogopite that may not be part of the primary MARID or PIC paragenesis (Fig. 3; Fitzpayne et al., 2018a, b). Sample dissolution was carried out at the University of Melbourne. First, the phlogopite separates (2–14 mg) were dissolved in a 3:1 mix of HF–HNO_3 (~48 h), followed by concentrated HNO_3 and 6 M HCl (~100 °C, ~24 h each). Chemical separation of Tl was carried out in the MAGIC laboratories at Imperial College London, following a two-step anion exchange column chromatography procedure described by Rehkamper and Halliday (1999), and modified by Nielsen et al. (2004). Three total procedural blanks yielded Pb at electronic background levels and <8 pg/g Tl.

The separated Tl fractions were diluted and doped with the NIST SRM981 lead isotopic standard to correct for instrumental mass bias. Thallium isotopic compositions were measured using a *Nu Instruments* HR MC-ICP-MS at Imperial College London. All sample analyses were conducted using sample-standard bracketing employing the NIST SRM997 Tl reference material, which is defined as $\varepsilon^{205}Tl = 0$. Samples were run at Pb/Tl ratios of 3–6 and contained 2 ng/g Tl. In order to minimize possible matrix

effects, concentrations of Pb and Tl in samples were matched to within 15% of their concentrations in the bracketing SRM997 standards. Therefore, all samples and standards were also diluted with a solution of 0.1 M HNO_3-0.1% H_2SO_4. The isotopic composition of a Tl solution standard from Sigma Aldrich, which has been measured by multiple laboratories ($\varepsilon^{205}Tl = -0.79 \pm 0.35$, 2 s.d., n = 187: Nielsen et al., 2017a), was analysed before samples were introduced and at the end of each run ($\varepsilon^{205}Tl = -1.0 \pm 0.3$, 2 s.d., n = 11; Supplementary Table 1).

Accuracy and precision were further assessed by measuring the Tl isotopic compositions of reference materials, including two separate dissolutions of USGS basaltic reference material BCR-2, and two CRPG/CNRS mica standards (Mica-Mg and Mica-Fe). Procedural duplicates of BCR-2 returned a combined average $\varepsilon^{205}Tl$ value of -2.4 ± 0.8 (external 2 s.d., n = 7), which is identical to published values (Supplementary Table 1; Brett et al., 2018; Prytulak et al., 2013). Both of the mica standards (Mica-Mg and Mica-Fe) also returned $\varepsilon^{205}Tl$ values (-0.2 ± 0.5 and -3.1 ± 0.9, respectively) that are within uncertainty of their published values (Supplementary Table 1: Brett et al., 2018).

The Tl contents of MARID and PIC phlogopite separates, as well as each of the dissolved standard reference materials, can be estimated by matching beam-size intensities during solution-mode MC-ICP-MS analyses (see Prytulak et al., 2013; Rehkamper and Halliday, 1999). Each of the standard reference materials analysed yielded Tl contents within uncertainty of previously reported values (Fig. 4; Supplementary Table 1; preferred values from Brett et al., 2018, and references therein).

4 Results

4.1 Thallium content in MARID and PIC phlogopite: *in situ* LA-ICP-MS vs solution-mode MC-ICPMS

All samples of PIC phlogopite display similar Tl contents via both *in situ* and solution-mode analytical methods except for sample FW-20, for which an order of magnitude more Tl (~5 μg/g; Table 2) was recorded when measured in solution than is indicated by *in situ* measurements (~0.4 μg/g; Table 1). Thallium contents in orangeite-derived MARID samples analysed *in situ* by Fitzpayne et al. (2018a) are also generally similar to those estimated by beam-matching during MC-ICPMS analysis in this study (Fig. 4). In contrast, kimberlite-derived MARID samples typically appear to contain less Tl when measured in solution (0.5–1.0 μg/g) than the average value reported from *in situ* phlogopite core trace element analyses (0.6–4.9 μg/g; Fig. 4; Fitzpayne et al., 2018a). The sample displaying the largest discrepancy, WES-2, contains phlogopite that is ubiquitously zoned and almost entirely replaced by poikilitic rims (Fig. 3a), likely due to interactions with its host kimberlite magma (Fitzpayne et al., 2018b).

Thallium abundances in both MARID and PIC phlogopite cores are not correlated with contents of either Al_2O_3 or K_2O, or abundances of other LILE (e.g., Rb; Fig. 5; data from Fitzpayne et al., 2018a). Furthermore, in contrast to the suggestion of Rader et al. (2018) for crustal mica, Tl concentrations in MARID and PIC phlogopite do not co-vary with Mg# [i.e. 100*Mg/(Mg+Fe)] (Fig. 5b).

4.2 Thallium isotopic composition of MARID and PIC phlogopite

Four of the PIC phlogopite samples have similar ε^{205}Tl values (–2.7 ± 0.8; external 2 s.d.; Table 2). However, the PIC sample with an unexpectedly high Tl content in solution analyses (FW-20; Fig. 3d) also has a much lower ε^{205}Tl value (–9.9 ± 0.6; external 2 s.d., n = 3). Phlogopite from kimberlite-hosted MARID xenoliths has an average ε^{205}Tl value of –2.5 ± 1.3 (external 2 s.d., n = 19; Table 2), which is within uncertainty of the average PIC phlogopite value. The two orangeite-derived MARID samples have ε^{205}Tl values of –3.6 ± 1.1 (external 2 s.d., n = 5) and –2.4 ± 0.8 (external 2 s.d., n = 4). There is no correlation between ε^{205}Tl and Tl content in the samples from this study (Fig. 6). There are no correlations between phlogopite ε^{205}Tl (this study) and the major element compositions of phlogopite cores analysed by Fitzpayne et al. (2018a; Supplementary Figure 1), or radiogenic isotopic compositions of coexisting clinopyroxene and amphibole determined by Fitzpayne et al. (2019; Supplementary Figure 2).

5 Discussion

In the following sections, the new Tl abundance and isotopic data are first considered in the context of potential kimberlite (i.e. entraining magma) contamination, before the incorporation of Tl into mantle micas is discussed. Thereafter, Tl abundances and isotope ratios are used to constrain the compositions of the parental PIC and MARID metasomatic agents, as well as the possible presence of recycled components in their sources. Finally, an explanation is sought for the light ε^{205}Tl value in PIC sample FW-20.

5.1 Homogeneous thallium isotopic compositions in MARID and PIC phlogopite

Although their mineral assemblages are unlike the depleted mantle, the ε^{205}Tl values of both MARID (–2.5 ± 1.3) and PIC phlogopite (–2.7 ± 0.8; Table 2) overlap with estimates of the mantle value (based on MORB data: –2.0 ± 1.0, 2 s.d.; Nielsen et al., 2017a). Each of these average values also overlaps with the ε^{205}Tl value of the bulk continental crust (–2.0 ± 0.5; Nielsen et al., 2005); however, the range in ε^{205}Tl observed in crustal micas (from –12 to +18; Rader et al., 2018) sharply contrasts with the homogeneity of MARID and PIC micas. Kimberlite infiltration of MARID samples has recently been suggested to cause the radiogenic isotopic compositions of MARID minerals to more closely resemble those of PIC rocks (Fitzpayne et al., 2019). If true, the measured MARID phlogopite Tl isotope ratios could be interpreted as either:

i. Complete equilibration between a pristine MARID end-member composition and the infiltrating kimberlite melt; or

ii. The result of partial equilibration of a MARID end-member composition with the entraining kimberlite, which both have mantle-like ε^{205}Tl values.

Solution-mode analyses of Tl contents in kimberlite-derived MARID bulk-phlogopite samples are generally lower than *in situ* data for phlogopite cores (Fig. 4; Table 2), and tend towards the Tl abundances of PIC phlogopite (i.e., phlogopite in equilibrium with kimberlite melt). This contrasts with the reference material measurements, all of which (n = 4) are consistent with reported values (Fig. 4; Supplementary Table 1). The difference between measurements of solution-mode and *in situ* Tl abundance are likely related to variable mixtures of pristine MARID phlogopite cores and secondary phlogopite rims that crystallised during interactions with kimberlite melts (Fig. 3a-b; Fitzpayne et al., 2018b, 2019). Some evidence for this can be found in the data

presented by Fitzpayne et al. (2018a, b), in which MARID phlogopite core analyses show generally higher Tl than their accompanying rims (Supplementary Figure 3).

Despite the variable development of kimberlite-related zonation in MARID phlogopite, both within and between samples (Fig. 3), MARID phlogopite ε^{205}Tl is surprisingly homogeneous (–2.5 ± 1.3; 2 s.d.; n = 21). Indeed, there is no analytically resolvable variation in ε^{205}Tl (see Table 2) between samples that show almost no zonation (e.g., sample AJE-2422; ε^{205}Tl = −2.0; Fig. 3b) and those that are extremely altered by kimberlite infiltration (e.g., sample WES-2; ε^{205}Tl = –1.6; Fig. 3a). Such intense kimberlite infiltration of sample WES-2, as depicted by its high proportion of phlogopite rims (Fig. 3a), may explain why the Tl content of the phlogopite separate from this sample is lower than in other MARID phlogopite samples, and so closely resembles the data (both *in situ* and by solution) for phlogopite in equilibrium with kimberlite melt (i.e. PIC phlogopite; Fig. 4; Table 2). Furthermore, the Tl isotopic compositions of the two orangeite-derived samples (–2.4 ± 0.8 and –3.6 ± 1.1; external 2 s.d.; Table 2), which have experienced no interaction with kimberlite melts (and limited interactions with orangeite melts, based on petrographic evidence: see Fitzpayne et al., 2018b), are also within uncertainty of the range of values in kimberlite-derived MARID phlogopite (Fig. 6). This suggests that, although MARID phlogopite might be variably affected by kimberlite infiltration, the original Tl isotope ratios in MARID phlogopite were similar to those of the entraining kimberlite melts (as given by PIC mica) with which they interacted. The ε^{205}Tl data for MARID phlogopite therefore most likely reflect mixing between "end-member" MARID and kimberlitic components with similar, mantle-like Tl isotopic compositions.

5.2 Thallium content in MARID phlogopite: crystal chemical

control?

The range of Tl contents in MARID mica samples from this study (i.e., 0.4–11.6 μg/g) is similar to previously reported data for crustal mica (Rader et al., 2018; Fig. 1, 5b). However, unlike Rader et al. (2018), this study has found no relationship between phlogopite Tl content and major oxide contents (Fig. 5), and it is therefore difficult to infer a crystal chemical control for Tl in mica. There is also no correlation between Tl and K in phlogopite (Fig. 5c), although K contents span a range of only about 1 wt.%. Rader et al. (2018) recently suggested that Tl incorporation into the mica structure is preferred at high Mg# (>80), and proposed that this was related to the larger ionic radius of Mg^{2+} compared to Fe^{2+}. There is no direct relationship between phlogopite Tl content and Mg# in the MARID and PIC suites from this study (Fig. 5b); however, the absolute range in Mg# is small, making it difficult to evaluate. Instead, the variability in the Tl content, as well as other major element abundances, of MARID phlogopite cores is probably caused by compositional heterogeneity in the parental MARID melt/fluid, or variable interaction between the parental MARID fluid and lithospheric wall-rocks (Fitzpayne et al., 2018a). These factors could also explain why MARID samples derived from the Newlands orangeite (~10 μg/g; Fig. 4, 5, 6) have higher Tl contents than those found in the Kimberley kimberlites (<5 μg/g), which are ~35 km away (e.g., Field et al., 2008). However, there is little difference between the *in situ* phlogopite core and solution-mode bulk phlogopite separate determinations of Tl abundance for orangeite-derived MARID samples (Fig. 4), indicating that orangeite interaction is itself unlikely to have caused this difference. Finally, the lack of correlation between phlogopite major and trace element compositions and their ε^{205}Tl values makes it unlikely that Tl isotopes are fractionated during the metasomatic interactions by which they formed, implying that MARID ε^{205}Tl values are representative of their parental metasomatic agent. This

may in part be due to the relatively hot mantle conditions (~960 °C: Konzett et al., 2014) at which MARID rocks are estimated to be formed.

5.3 Can Tl isotopes trace recycled components in mantle-derived micas?

5.3.1 Equilibrium between PIC and kimberlite melts, and the composition of the kimberlite melt source

Previous geochemical and isotopic studies have proposed a genetic link between PIC rocks and kimberlites (Fitzpayne et al., 2018a, b, 2019; Grégoire et al., 2002). The Tl content and Tl isotopic ratio of PIC phlogopite should therefore be in equilibrium with those of kimberlitic melts. The Tl abundances in PIC phlogopite (0.42–0.46 μg/g; Table 1) are similar to those of bulk-rock analyses of the Kimberley kimberlites (0.08–0.65 μg/g Tl: Muramatsu, 1983). These values imply a range in empirical Tl partition coefficients between PIC phlogopite and kimberlites ($^{phl/kimb}D_{Tl}$ from 0.6 to 5.8) that is similar to published experimental data for other silica-undersaturated melts ($^{phl/melt}D_{Tl}$ = 3.0–5.2 for nepheline basanites: Adam and Green, 2006), potentially supporting a genetic link between kimberlite melts and PIC rocks.

The use of partition coefficients can be extended to examine the Tl content of a kimberlite melt in equilibrium with its mantle source. To the authors' knowledge, no bulk partition coefficient data have been published for Tl between peridotites and silica-undersaturated melts. Thallium (i.e. Tl^+) exhibits similar behaviour to alkali metal ions (K^+, Rb^+, Cs^+). Values for peridotite-carbonatite partitioning coefficients ($^{peridotite/melt}D$) are almost identical for Rb and Cs (~0.003; e.g., Dasgupta et al., 2009). This value is therefore used to approximate that of $^{peridotite/melt}D_{Tl}$. The primitive mantle (here used as an approximation of the undepleted, asthenospheric mantle) has an estimated Tl content

of 0.0035 μg/g (McDonough and Sun, 1995), whereas the depleted mantle contains an order of magnitude less Tl (0.00038 μg/g; Salters and Stracke, 2004). Bulk-rock samples of peridotite also have low Tl contents (<0.00355 μg/g; Nielsen et al., 2015; Wang et al., 2018). In an equilibrium partial melting scenario, with a melt fraction of between 0.5 and 1.0% (see discussion in Soltys et al., 2018), a primary kimberlite melt sourced from the convective mantle should contain between 0.03 and 0.44 μg/g Tl, which overlaps the range of Tl contents in the Kimberley kimberlites (0.08–0.65 μg/g: Muramatsu, 1983). This similarity might suggest that kimberlites are formed by partial melting of the convective mantle in the presence of CO_2, consistent with some experimental studies (e.g., Dasgupta et al., 2009; Stamm and Schmidt, 2017). To the authors' knowledge, Tl isotope data have not been collected for kimberlites; thus, the proposed equilibrium between PIC and kimberlites permits the use of PIC ε^{205}Tl values as a proxy for those of kimberlites.

5.3.2 Recycled components in kimberlite melts?

Some stable isotope studies on kimberlites have indicated that they have signatures broadly similar to reported mantle values, for example carbonate δ^{13}C (median value of –5.3 ‰: Giuliani et al., 2014b) and olivine δ^{18}O (see Giuliani et al., *in press*). The ε^{205}Tl values in PIC phlogopite, here employed as a proxy for kimberlite melt compositions, are also similar to mantle values (–2.7 ± 0.8; 2 s.d., n = 4). However, O isotopic compositions in kimberlite-derived xenoliths sometimes exhibit disequilibrium, perhaps as a result of interactions with the entraining kimberlite melt. Examples of this phenomenon have been found in wehrlites associated with kimberlite metasomatism (e.g., Fitzpayne et al., *in press*; Rehfeldt et al., 2008), as well as mantle polymict breccias (Zhang et al., 2000, 2001), and some superdeep xenoliths (Deines and

Haggerty, 2000). Furthermore, Fitzpayne et al. (*in press*) showed that wehrlites — which appear to be products of kimberlite melt metasomatism — display high $\delta^{15}N$ values (+5.9 ‰), similar to continental sediments (+7.2 ± 3.3; Cartigny and Marty, 2013). Perovskite from the Kimberley kimberlites also displays an initial Sr isotope ratio ($^{87}Sr/^{86}Sr_i$ = 0.7043–0.7046) that is generally higher than other coeval kimberlites on the Kaapvaal craton (0.7032–0.7045; Woodhead et al., 2009). Finally, the few Pb isotope studies on southern African Cretaceous kimberlites have found high $^{206}Pb/^{204}Pb$ ratios consistent with a kimberlite source containing a HIMU component (Collerson et al., 2010; Janney and Bell, 2017; Smith, 1983), which could relate to either subducted oceanic crust (Zindler et al., 1982), carbonate-rich sediments (Castillo, 2015), or delaminated, carbonate-metasomatised SCLM (Weiss et al., 2016). Overall, the combined stable and radiogenic isotope evidence support the incorporation of a recycled component into the melt source of the Kimberley kimberlites.

The mantle-like $\varepsilon^{205}Tl$ values of PIC phlogopite indicate that any recycled contributions to PIC (and hence, kimberlite melt) genesis must either closely resemble the Tl-$\varepsilon^{205}Tl$ systematics of the mantle, or be incorporated in sufficiently small amounts that the mantle source retains a low Tl abundance as well as an $\varepsilon^{205}Tl$ value close to –2 ± 1. To constrain the possible contribution of recycled components (continental crust, altered oceanic crust, pelagic clay, and ferromanganese sediments) to PIC genesis, a mass balance mixing model in Tl-$\varepsilon^{205}Tl$ space was constructed between these crustal lithologies and that of the mantle (0.0035 μg/g Tl: McDonough and Sun, 1995; $\varepsilon^{205}Tl$ = –2.0: Nielsen et al., 2006a, 2017a). For each crustal component, ranges in Tl content and $\varepsilon^{205}Tl$ were selected from previously reported values:

- Low temperature-altered oceanic crust (AOC): 0.04–0.15 μg/g Tl; $\varepsilon^{205}Tl$ = –9 to –16 (Coggon et al., 2014; Nielsen et al., 2006a);

- Pelagic clay: 0.5–1.5 μg/g Tl; ε^{205}Tl = +2.5 to +5.0 (Rehkamper et al., 2004);
- Ferromanganese sediment: 30–150 μg/g Tl; ε^{205}Tl = +10 to +15 (Rehkamper et al., 2002);
- Continental crust: 0.5–1.6 μg/g Tl (Rudnick and Gao, 2014); ε^{205}Tl = –2.0 ± 0.5 (Nielsen et al., 2005);
- High temperature-AOC: 0.005 μg/g Tl; ε^{205}Tl = –2 (Nielsen et al., 2006a).

Notably, pelagic clay has an ε^{205}Tl value distinct from the continental crust, despite pelagic clays likely being predominantly composed of continental sediments. The positive ε^{205}Tl values in pelagic clays have been related to the adsorption of authigenic Fe-Mn oxyhydroxides onto these clays (Rehkamper et al., 2004). From a mass balance perspective, adding to the primitive mantle even 1% of any of the first three components listed above will cause a shift of >1 epsilon unit (i.e., outside of the range of mantle ε^{205}Tl = –2 ± 1; Fig. 7). Similarly, the addition to the primitive mantle of 1% of a continental crust component creates a mixture with a Tl content of 0.018 μg/g: a kimberlitic partial melt derived from 0.5-1.0% melting of such a source would contain 1.4–2.3 μg/g Tl, much greater than any reported bulk-rock kimberlite data. The similarity between the Tl-ε^{205}Tl of the primitive mantle and high temperature-altered oceanic crust make this the only plausible recycled component that might have been incorporated into PIC rocks (and kimberlites), because the mantle-like ε^{205}Tl values of PIC rocks cannot accommodate significant input from any other recycled material. Moreover, kimberlite bulk-rock Tl contents, in combination with previously reported partitioning data, appear to be consistent with partial melting of a carbonated, low-Tl mantle source (either the convective mantle, or high temperature-AOC).

5.3.3 Identifying recycled components in MARID rocks

It is likely that MARID parental melts/fluids contain more Tl than kimberlites, based on the relative Tl contents of MARID and PIC mica (Table 1) and assuming that similar mica-melt Tl partition coefficients can be employed, i.e. the MARID parental melt is also silica-undersaturated (e.g., Dawson and Smith, 1977; Fitzpayne et al., 2018a; Sweeney et al., 1993). Combining the same $^{phl/melt}D_{Tl}$ values (0.6–5.8) with the Tl contents of primary MARID phlogopite cores (0.6–11.6 μg/g; Table 1) leads to a wide range in the possible Tl contents of MARID parental melts (0.1–19.4 μg/g). Moreover, assuming that this parental melt also contains a carbonate component (based on experimental data: e.g., Sweeney et al., 1993), it can be assumed that the MARID parental melt is derived from a similar, carbonated lherzolite composition at high pressure to PIC rocks (see previous section). Thus, assuming again a low degree of melting (0.5–1.0%), the same $^{peridotite/melt}D_{Tl}$ value (0.003) can be employed to show that the source assemblage to MARID parental melts contains between 0.0008 and 0.25 μg/g of Tl. This range includes the values employed earlier for the Tl content of the mantle (0.00038–0.0035 μg/g) as well as values up to ~70 times greater than that of the primitive, undepleted mantle (0.0035 μg/g; McDonough and Sun, 1995).

As demonstrated by the PIC samples from this study, the mantle-like $\varepsilon^{205}Tl$ values in MARID phlogopite at first also suggest that no recycled component is required within the source of MARID parental melts. This contrasts with evidence that "primary" MARID minerals (i.e. before late-stage metasomatism) have "enriched mantle" radiogenic isotopic compositions (i.e. $^{87}Sr/^{86}Sr_i = 0.711$; $\varepsilon Nd_i = -11$; $^{206}Pb/^{204}Pb = 17.33$), suggestive of the presence of recycled components in the source of their metasomatic agent (Fitzpayne et al., 2019). A recycled component in MARID rocks

(and related lherzolites) is supported by recent stable isotope evidence, although some uncertainty remains as to the identity of the recycled component, potentially being related to continental crust/sediments, or alternately low or high temperature-altered oceanic crust (e.g., Banerjee et al., 2015, 2018; Fitzpayne et al., *in press*). A two-step mass balance mixing model is constructed here for MARID rocks. The first step is used to determine which recycled components might be mixed together while preserving a range in ε^{205}Tl values resembling that of MARID rocks. The second step examines how much of such a mixed recycled component can be combined with a primitive mantle composition to generate a mantle source containing between 0.0008 and 0.25 µg/g Tl (i.e., given by MARID melts in equilibrium with a peridotite source, using $^{peridotite/melt}D_{[Rb, Cs, Tl]}$ from Dasgupta et al., 2009).

High Tl contents and mantle-like ε^{205}Tl values in MARID phlogopite are remarkably similar to the characteristics of the continental crust (Fig. 8), indicating perhaps that MARID genesis is heavily influenced by continental material. Therefore, mass balances were initially calculated between the continental crust and other recycled components (see section 5.3.2) to determine which other crustal components might be incorporated without causing a shift in ε^{205}Tl value beyond the range observed in MARID samples in this study (–3.9 to –1.6; Table 2). These calculations are shown graphically in Fig. 8, and demonstrate how mixing 0–55% of a low temperature-AOC component with continental sediment results in an ε^{205}Tl range (–3.9 to –1.5) almost identical to that found in MARID samples. In contrast, very little (if any) pelagic clay or Fe-Mn sediment can be mixed with continental crust to be inferred as a likely explanation for MARID ε^{205}Tl compositions (Fig. 8).

In the second step of the mixing model, mixtures are calculated for varying proportions of the hybrid low temperature-AOC/continental crust component and the

primitive mantle, to examine how much crustal material might be incorporated to create Tl contents up to 0.25 µg/g. It is important to note again that high temperature-altered oceanic crust contains 0.005 µg/g Tl, and has $\varepsilon^{205}Tl \approx -2$ (Nielsen et al., 2006a), making this component almost identical to the model primitive mantle composition used in Fig. 7 and 8. It is therefore not possible to quantify the relative amounts of primitive mantle and high temperature-altered oceanic crust that might contribute to MARID genesis using only the Tl isotopic data presented in this study. Nevertheless, the mixing calculations performed here show that incorporating 1–30% or 1–50% of the mixed low temperature-AOC + continental crust component or of continental crust alone, respectively, into a primitive mantle composition (and/or high temperature-AOC; Fig. 8) results in Tl contents of up to 0.25 µg/g, while maintaining a range in $\varepsilon^{205}Tl$ (–3.9 to –1.5) that resembles the range observed in MARID phlogopite (Table 2: –3.9 to –1.6).

The stable (N-O-S) isotopic data presented for MARID and related lherzolite minerals (Fitzpayne et al., *in press*, and references therein) are somewhat inconclusive in identifying recycled components in metasomatised rocks. Indeed, MARID source components can be variably related to continental crust/sediment (low $\delta^{34}S$, high $\delta^{15}N$), low temperature-AOC (low $\delta^{34}S$), or high temperature-AOC (low $\delta^{18}O$, high $\delta^{15}N$). The Tl isotopic data presented in this study and the accompanying models might support a model wherein the MARID parental metasomatic agent is produced by melting of a primitive mantle composition potentially also including a high temperature-AOC component of identical Tl-$\varepsilon^{205}Tl$ composition, mixed with 1–30% of a hybrid component containing both continental crust/sediments and low temperature-AOC (Fig. 8) or 1–50% of continental crust alone.

It remains to be shown whether such a mixed recycled source could melt to produce a MARID parental melt. Fitzpayne et al. (2018a) used MARID mineral

geochemistry and reconstructed bulk-rock compositions to infer that MARID rocks were crystallised in an open system from an ultrapotassic and hydrous melt, which might have a wide range in Mg# (51–77). Recent experiments by Wang et al. (2017) examined the melting behaviour of a combined continental crustal metasediment + depleted oceanic peridotite source at 2–3 GPa and 1000–1100 °C. The hybridized melts have high K_2O contents (3.4–5.1 wt.%), with a wide range in Mg# (between 48 and 73). This similarity to the predicted MARID parental melt composition supports a mixed recycled component in the source of MARID rocks.

In summary, the combination of unusual and apparently decoupled stable isotopic compositions might best relate to a MARID parental melt source that comprises a mixed oceanic crust + continental sediment component as well as peridotitic material. Melting experiments on oceanic peridotite + continental crust compositions have derived melt compositions that closely resemble those predicted for MARID parental metasomatic agents, lending support to a model for MARID genesis requiring a recycled contribution.

5.4 Anomalously low ε^{205}Tl in PIC sample FW-20

In contrast to the other four PIC samples, sample FW-20 has a much lower ε^{205}Tl of –9.9 ± 0.6 (2 s.d.) than the reported mantle range. This sample was originally characterised as a PIC sample using the suggested characteristics of Grégoire et al. (2002); however, it appears that this sample is slightly different to both MARID and PIC both in terms of its geochemistry (e.g., phlogopite Al_2O_3 content: FW-20: 11.1 ± 0.2 wt.%, 1 s.d., n = 9; MARID: 9.9 ± 0.6 wt.%, n = 210; PIC: 12.0 ± 0.5 wt.%, n = 42; Fig. 5a; Fitzpayne et al., 2018a) and its radiogenic isotope systematics (FW20 εHf = –

5.8; MARID εHf between –17.9 and –8.5; PIC εHf between +2.2 and +2.5; Supplementary Figure 2; Fitzpayne et al., 2019).

Figure 4 shows that the Tl abundance estimated for the mineral separate digestion of sample FW-20 (~4.9 μg/g) is an order of magnitude greater than the abundance determined *in situ* (0.46 ± 0.38 μg/g; 2s.d., n = 6; Fitzpayne et al., 2018a). The conformity of Tl concentrations in standard reference materials relative to their published values (Fig. 4) and the lack of Tl contamination in total procedural blanks together suggest that variation between *in situ* and solution analyses are real phenomena. While other discrepancies between analytical methods have been explained by kimberlite infiltration, such alteration cannot be invoked as the cause of increased Tl in sample FW-20 due to the low abundances of Tl in the Kimberley kimberlites (0.25 ± 0.23 μg/g: Muramatsu, 1983) and other PIC samples (~0.4 μg/g; Table 2). Moreover, phlogopite porphyroclasts in sample FW-20 are remarkably free of inclusions, ruling out other high-Tl minerals as the cause of the unusual ε^{205}Tl in this sample.

Sample FW-20 exhibits a porphyroclastic texture (Fig. 3d; Fitzpayne et al., 2019), wherein phlogopite has a bimodal size distribution separating sheared and recrystallised grains (<50 μm) from larger, undeformed porphyroclasts (>100 μm). Larger size fractions (>250 μm) were also employed during mineral separation, and great care was taken (as for other PIC samples) in ensuring that separated grains were single porphyroclasts and not larger aggregates of finer-grained phlogopite neoblasts. Sampling bias therefore seems an unlikely explanation, as this would also occur in other MARID and PIC samples, and this discrepancy therefore remains unexplained.

Although sheared and deformed textures are common in PIC samples (e.g., Fig. 3c; Dawson and Smith, 1977; Fitzpayne et al., 2018a; Grégoire et al., 2002), sample FW-20 appears to be an extreme example. Indeed, this sample contains unusual

serpentine + talc rinds replacing large (~300 μm) clinopyroxene porphyroclasts (Fig. 9a) that are not observed in other PIC samples. Soltys et al. (2016) interpreted similar replacement features in a wehrlite xenolith from Bultfontein as the result of alteration by crustal fluids during or after kimberlite emplacement into the crust. The occurrence of mineral inclusions in clinopyroxene such as chromatite ($CaCrO_4$; Fig. 9b), which must contain oxidised Cr^{6+} and S^{6+} species (Supplementary Table 2), further attests to fluid interactions within an oxidised, likely near-surface environment. Low temperature-alteration has previously been suggested as an explanation for $\varepsilon^{205}Tl$ values less than –2 in altered oceanic basalts, owing to Tl partitioning into either biogenic pyrite (Coggon et al., 2014) or into alkali-rich replacement products such as clay minerals (Nielsen et al., 2006a). Such alteration might explain the Tl isotopic composition of sample FW-20 ($\varepsilon^{205}Tl = –9.9$), and evidence for similar late-stage, low temperature-alteration has been found in vein carbonates in kimberlite-derived xenoliths, based on positive $\delta^{13}C$-$\delta^{18}O$ excursions from typical mantle values (Fitzpayne et al., 2018b). However, the absence of chlorite or other evidence for replacement or alteration of phlogopite in sample FW-20 argues against low temperature-alteration as the cause of the low $\varepsilon^{205}Tl$ value in this sample. Moreover, the fact that variations are observed in all radiogenic isotope systems (including εHf_i) in clinopyroxene from sample FW-20 compared with other PIC samples (Supplementary Figure 2; Fitzpayne et al., 2019) makes near-surface fluid interactions unlikely to be the cause of variable isotopic compositions in sample FW-20.

The non-mantle $\varepsilon^{205}Tl$ value in sample FW-20 might instead be the result of equilibrium isotope fractionation between phlogopite and another Tl-bearing phase. The mineral separates analysed by Rader et al. (2018) show that sulfides coexisting with micas appear to preferentially host the heavy ^{205}Tl isotope, perhaps suggesting that equilibrium fractionation between sulfides and phlogopite in FW-20 could be the cause

of low ε^{205}Tl in this sample. However, sulfides in sample FW-20 are no more or less abundant compared to other PIC or MARID samples, nor is the sulfide assemblage (typically pentlandite, chalcopyrite, heazlewoodite) any different. Finally, the trace element data reported by Fitzpayne et al. (2018a) demonstrate that Tl is much less abundant (<<0.1 μg/g) in all other constituent MARID and PIC phases (i.e., amphibole, clinopyroxene, rutile, and ilmenite) compared to mica, further ruling out any role for equilibrium isotope fractionation.

Kinetic isotope fractionation has previously been suggested as the cause of non-mantle ε^{205}Tl values in volcanic samples due to degassing (e.g., Baker et al., 2009), or during Tl diffusion between metal and sulfide phases in meteorites (Nielsen et al., 2006c). It is possible that the extreme shearing and recrystallisation experienced by sample FW-20, as evidenced by its unusual petrographic features relative to other PIC samples (Fig. 3, 9), is the cause of its radiogenic isotope features (Supplementary Figure 2). However, due to the difference in radiogenic isotope composition between sample FW-20 (e.g., $^{87}Sr/^{86}Sr_i$ = 0.7049: Fitzpayne et al., 2019) and the Bultfontein kimberlite ($^{87}Sr/^{86}Sr_i$ = ~0.7043: e.g., Giuliani et al., 2017) from which it is derived, it is unlikely that a kimberlitic melt is responsible for causing kinetic isotope fractionation. Some sheared mantle samples derived from kimberlites show evidence of fluid/melt metasomatism that is almost contemporaneous with kimberlite magmatism, and occurring at mantle depths (e.g., Giuliani et al., 2013a, 2013b). It is therefore speculated that such shearing and metasomatism also affected sample FW-20 shortly before/during xenolith entrainment, resulting in kinetic Tl isotope fractionation. It is notable that sample FW-20 has an ε^{205}Tl value that is within the previously reported ε^{205}Tl range for micas in crustal rocks ($-12 < \varepsilon^{205}Tl < +18$; Rader et al., 2018; Fig. 6). Kinetic fractionation of Tl isotopes could therefore also explain some of the ε^{205}Tl variations in

crustal micas that equilibrated at different conditions (e.g., granulites, carbonatites; Rader et al., 2018). The unusual isotopic compositions occurring in sample FW-20, and by association other samples that have experienced intense melt metasomatism during kimberlite magmatism, warrant further investigation into the many effects accompanying kimberlite magmatism upon the lithospheric mantle.

6 Conclusions

This study presents the first Tl isotopic analyses of mantle-derived phlogopite in 26 MARID and PIC xenoliths from the Kimberley kimberlites (South Africa) and the nearby Newlands orangeite. Despite the contrasting genetic models previously proposed for these rocks, all but one of the MARID and PIC samples has an ε^{205}Tl value consistent with estimates of the mantle value, reinforcing previous estimates thereof. Recent suggestions of a genetic link between PIC rocks and kimberlite melts imply that kimberlites also have mantle-like ε^{205}Tl values, at least in the Kimberley area. Mass balance calculations indicate that high temperature-altered oceanic crust is the only possible recycled component that might be incorporated into the kimberlite melt source region. Alternatively, models employing published trace element partitioning coefficients suggest that kimberlite melt Tl contents could be the result of low degree (~0.5%) equilibrium partial melting of a carbonated mantle peridotite source at high pressure, consistent with some experimental studies.

MARID samples also have mantle-like ε^{205}Tl values. These data support the possibility that MARID genesis does not require a recycled contribution, although such a conclusion is contradicted by recently published radiogenic and stable N-O isotopic

data. The range in observed Tl contents in MARID phlogopite leads to a correspondingly wide range in the Tl content of its modelled mantle source. Further mass balance modelling suggests that mixing of the undepleted mantle with 1–30% of a hybrid low temperature-altered oceanic crust + continental crust component or 1–50% of continental crust alone could be accommodated by the Tl-ε^{205}Tl systematics required for a melt parental to MARID rocks. This supports evidence of a mixed recycled component in MARID rocks and related lherzolites from previous radiogenic and stable isotope investigations (Fitzpayne et al., 2019, *in press*). Combining traditional isotope systems with Tl therefore offers a fruitful avenue of further research in the study of mantle metasomatic processes.

Finally, one PIC sample (FW-20) has an anomalously low ε^{205}Tl value (–9.9 ± 0.6 2s.d.), and also displays unusual petrographic, geochemical, and radiogenic isotope features compared to other PIC samples. Low temperature-alteration has been ruled out based on petrographic grounds (e.g., absence of chlorite). Rather, these features most strongly suggest that this sample experienced kinetic isotope effects as a result of the intense shearing/recrystallisation event that created its unique texture at mantle depths. It is envisaged that such kinetic isotope effects occurred shortly before/during xenolith entrainment and kimberlite melt infiltration.

The Tl contents of mantle-derived MARID and PIC phlogopite (>0.2 μg/g) are much greater than estimates of the mantle Tl abundance (<0.003 μg/g). MARID and PIC compositions have previously been related to other metasomatised mantle samples (e.g., lherzolites), suggesting that such Tl-rich phlogopite may not be restricted to rare MARID and PIC samples within the lithospheric mantle. It is therefore suggested that, despite their exotic, metasomatic nature, the restricted ε^{205}Tl values in most MARID

and PIC samples (–3.9 to –1.6) support previous estimates of the mantle's Tl isotopic composition ($\varepsilon^{205}Tl \sim -2$).

Acknowledgements

We thank De Beers Consolidated Mines, the J. J. Gurney Upper Mantle Room Collection (University of Cape Town), and Simon Shee for kindly providing access to the studied samples, and Jock Robey for his assistance during fieldwork in the Kimberley region. We also wish to thank Barry Coles for his help throughout the analytical sessions, as well as Katharina Kreissig, Roland Maas, and Serene Paul for their assistance and support in the clean labs. This manuscript benefited from the constructive reviews of two anonymous reviewers, as well as the efficient editorial handling of Catherine Chauvel. AF's PhD research has been supported by the Gilbert Rigg Scholarship from the University of Melbourne, and this project was specifically supported by further funding from the George Sweet and Baragwanath scholarships, as well as a Science Abroad Travelling Scholarship, all from the University of Melbourne. This manuscript was written with the support of the Albert Shimmins Fund from the University of Melbourne. This is publication 48 from the Kimberlites and Diamonds Research Group (https://kimberlitesdiamonds.org/).

References

Adam, J., Green, T., 2006. Trace element partitioning between mica- and amphibole-bearing garnet lherzolite and hydrous basanitic melt: 1. Experimental results and

the investigation of controls on partitioning behaviour. Contributions to Mineralogy and Petrology, 152: 1-17

Allsopp, H. L., Barrett, D. R., 1975. Rb-Sr age determination on South African kimberlite pipes. Physics and Chemistry of the Earth, 9: 605-617

Alt, J. C., Shanks, W. C., 2011. Microbial sulfate reduction and the sulfur budget for a complete section of altered oceanic basalts, IODP Hole 1256D (eastern Pacific). Earth and Planetary Science Letters, 310: 73-83

Aoki, K.-I., 1974. Phlogopites and potassic richterites from mica nodules in South African kimberlites. Contributions to Mineralogy and Petrology, 48: 1-7

Aulbach, S., Griffin, W. L., Pearson, N. J., O'Reilly, S. Y., 2013. Nature and timing of metasomatism in the stratified mantle lithosphere beneath the central Slave craton (Canada). Chemical Geology, 352: 153-169

Baker, R. G. A., Rehkamper, M., Hinkley, T. K., Nielsen, S. G., Toutain, J. P., 2009. Investigation of thallium fluxes from subaerial volcanism – implications for the present and past mass balance of thallium in the oceans. Geochimica et Cosmochimica Acta, 73: 6340-6359

Banas, A., Stachel, T., Phillips, D., Shimizu, N., Viljoen, K. S., Harris, J. W., 2009. Ancient metasomatism recorded by ultra-depleted garnet inclusions in diamonds from De Beers pool, South Africa. Lithos, 112: 736-746

Banerjee, S., Kurtis Kyser, T., Mitchell, R. H., 2015. Nitrogen isotopic compositions and concentrations in MARID xenoliths. Chemical Geology, 391: 83-89

Batley, G. E., Florence, T. M., 1975. Determination of thallium in natural waters by anodic stripping voltammetry. Electroanalytical Chemistry and Interfacial Electrochemistry, 61: 205-211

Bea, F. P., Pereira, M. D., Stroh, A., 1994. Mineral/leucosome trace element partitioning in a peraluminous migmatite (a laser ablation-ICP-MS study). Chemical Geology, 117: 291-312

Brett, A., Prytulak, J., Hammond, S. J., Rehkamper, M., 2018. Thallium mass fraction and stable isotope ratios of sixteen geological reference materials. Geostandards and Geoanalytical Research, 42(3), 339-360.

Bussweiler, Y., Pearson, D. G., Stachel, T., Kjarsgaard, B. A., 2018. Cr-rich megacrysts of clinopyroxene and garnet from Lac de Gras kimberlites, Slave Craton, Canada – implications for the origin of clinopyroxene and garnet in cratonic lherzolites. Mineralogy and Petrology, 112(S2): 583-596

Carswell, D. A., 1975. Primary and secondary phlogopites and clinopyroxenes in garnet lherzolite xenoliths. Physics and Chemistry of the Earth, 9: 417-429

Cartigny, P., Marty, B., 2013. Nitrogen isotopes and mantle geodynamics: the emergence of life and the atmosphere-crust-mantle connection. Elements, 9: 359-366

Castillo, P. R., 2015. The recycling of marine carbonates and sources of HIMU and FOZO ocean island basalts. Lithos, 216: 254-263

Coggon, R. M., Rehkamper, M., Atteck, C., Teagle, D. A. H., Alt, J. C., Cooper, M. J., 2014. Controls on thallium uptake during hydrothermal alteration of the upper ocean crust. Geochimica et Cosmochimica Acta, 144: 25-42

Collerson, K. D., Williams, Q., Ewart, A. E., Murphy, D. T., 2010. Origin of HIMU and EM-1 domains sampled by ocean island basalts, kimberlites and carbonatites: the role of CO_2-fluxed lower mantle melting in thermochemical upwellings. Physics of the Earth and Planetary Interiors, 181: 112-131

Dasgupta, R., Hirschmann, M. M., McDonough, W. F., Spiegelman, M., Withers, A. C., 2009. Trace element partitioning between garnet lherzolite and carbonatite at 6.6 and 8.6 GPa with applications to the geochemistry of the mantle and of mantle-derived melts. Chemical Geology, 262: 57-77

Dawson, J. B., Smith, J. V., 1977. The MARID (mica-amphibole-rutile-ilmenite-diopside) suite of xenoliths in kimberlite. Geochimica et Cosmochimica Acta, 41: 309-333

Deines, P., Haggerty, S. E., 2000. Small-scale oxygen isotope variations and petrochemistry of ultradeep (>300 km) and transition zone xenoliths. Geochimica et Cosmochimica Acta, 64(1): 117-131

Erlank, A. J., Finger, L. W., 1970. The occurrence of potassic richterite in a mica nodule from the Wesselton kimberlite, South Africa. Carnegie Institute Washington, Year Book, 68: 320-324

Erlank, A. J., Waters, F. G., Hawkesworth, C. J., Haggerty, S. E., Allsopp, H. L., Rickard, R. S., Menzies, M., 1987. Evidence for mantle metasomatism in peridotite nodules from the Kimberley pipes, South Africa. Mantle metasomatism, pp. 221-311

Farquhar, J., Wu, N., Canfield, D. E., Oduro, H., 2010. Connections between sulfur cycle evolution, sulfur isotopes, sediments, and base metal sulfide deposits. Economic Geology, 105: 509-533

Field, M., Stiefenhofer, J., Robey, J., Kurszlaukis, S., 2008. Kimberlite-hosted diamond deposits of southern Africa: a review. Ore Geology Reviews, 34(1): 33-75

Fitzpayne, A., Giuliani, A., Harris, C., Thomassot, E., Cheng, C., Hergt, J., *in press*. Evidence for subduction-related signatures in the southern African lithosphere

from the N-O isotopic composition of metasomatic mantle minerals. Geochimica et Cosmochimica Acta

Fitzpayne, A., Giuliani, A., Hergt, J., Janney, P., Phillips, D., 2019. Progressive metasomatism of the mantle by kimberlite melts: Sr-Nd-Hf-Pb isotope compositions of MARID and PIC minerals. Earth and Planetary Science Letters, 509: 15-26

Fitzpayne, A., Giuliani, A., Hergt, J., Phillips, D., Janney, P., 2018a. New geochemical constraints on the origins of MARID and PIC rocks: implications for mantle metasomatism and mantle-derived potassic magmatism. Lithos, 318-319: 478-493

Fitzpayne, A., Giuliani, A., Phillips, D., Hergt, J., Woodhead, J. D., Farquhar, J., Fiorentini, M. L., Drysdale, R. N., Wu, N., 2018b. Kimberlite-related metasomatism recorded in MARID and PIC mantle xenoliths. Mineralogy and Petrology, 112(S1): 71-84

Foley, S. F., 1992. Vein-plus-wall-rock melting mechanisms in the lithosphere and the origin of potassic alkaline magmas. Lithos, 28(3-6): 435-453

Giuliani, A., Fiorentini, M. L., Martin, L. A. J., Farquhar, J., Phillips, D., Griffin, W. L., LaFlamme, C., 2016. Sulfur isotope composition of metasomatised mantle xenoliths from the Bultfontein kimberlite (Kimberley, South Africa): contribution from subducted sediments and the effect of sulfide alteration on S isotope systematics. Earth and Planetary Science Letters, 445: 114-124

Giuliani, A., Kamenetsky, V. S., Kendrick, M. A., Phillips, D., Goemann, K., 2013a. Nickel-rich metasomatism of the lithospheric mantle by pre-kimberlitic alkali-S-Cl-rich C-O-H fluids. Contributions to Mineralogy and Petrology, 165: 155-171

Giuliani, A., Phillips, D., Fiorentini, M. L., Kendrick, M. A., Maas, R., Wing, B. A., Woodhead, J. D., Bui, T. H., Kamenetsky, V. S., 2013b. Mantle oddities: a sulphate fluid preserved in a MARID xenolith from the Bultfontein kimberlite (Kimberley, South Africa). Earth and Planetary Science Letters, 376: 74-86

Giuliani, A., Phillips, D., Kamenetsky, V. S., Fiorentini, M. L., Farquhar, J., Kendrick, M. A., 2014b. Stable isotopes (C, O, S) compositions of volatile-rich minerals in kimberlites: a review. Chemical Geology, 374-375: 61-83

Giuliani, A., Phillips, D., Maas, R., Woodhead, J. D., Kendrick, M. A., Greig, A., Armstrong, R. A., Chew, D., Kamenetsky, V. S., Fiorentini, M. L., 2014a. LIMA U-Pb ages link lithospheric mantle metasomatism to Karoo magmatism beneath the Kimberley region, South Africa. Earth and Planetary Science Letters, 401: 132-147

Giuliani, A., Phillips, D., Woodhead, J. D., Kamenetsky, V. S., Fiorentini, M. L., Maas, R., Soltys, A., Armstrong, R. A., 2015. Did diamond-bearing orangeites originate from MARID-veined peridotites in the lithospheric mantle? Nature Communications, 6: 6837

Grégoire, M., Bell, D., le Roex, A., 2002. Trace element geochemistry of phlogopite-rich mafic mantle xenoliths: their classification and their relationship to phlogopite-bearing peridotites and kimberlites revisited. Contributions to Mineralogy and Petrology, 142(5): 603-625

Grégoire, M., Bell, D. R., le Roex, A. P., 2003. Garnet lherzolites from the Kaapvaal craton (South Africa): Trace element evidence for a metasomatic history. Journal of Petrology, 44(4): 629-657

Gurney, J. J., Harte, B., 1980. Chemical variations in upper mantle nodules from southern African kimberlites. Philosophical Transactions of the Royal Society of London A, 297: 273-293

Gurney, J. J., Harte, B., Cox, K. G., 1975. Mantle xenoliths in the Matsoku kimberlite pipe. Physics and Chemistry of the Earth, 9: 507-523

Haggerty, S. E., 1983. The mineral chemistry of new titanates from the Jagersfontein kimberlite, South Africa: implications for metasomatism in the upper mantle. Geochimica et Cosmochimica Acta, 47: 1833-1854

Hamilton, M. A., Pearson, D. G., Stern, R. A., Boyd, F. R., 1998. Constraints on MARID petrogenesis: SHRIMP II U-Pb zircon evidence for pre-eruption metasomatism at Kampfersdam. Paper presented at the 7th International Kimberlite Conference, Extended Abstracts, Cape Town

Harte, B., Cox, K. G., Gurney, J. J., 1975. Petrography and geological history of upper mantle xenoliths from the Matsoku kimberlite pipe. Physics and Chemistry of the Earth, 477-506

Harte, B., Hunter, R. H., Kinny, P. D., 1993. Melt geometry, movement and crystallization, in relation to mantle dykes, veins and metasomatism. Philosophical Transactions of the Royal Society of London A 342: 1-21

Herzberg, C., 2004. Geodynamic information in peridotite petrology. Journal of Petrology, 45(12): 2507-2530

Hettmann, K., Marks, M. A. W., Kreissig, K., Zack, T., Wenzel, T., Rehkamper, M., Jacob, D. E., Markl, G., 2014. The geochemistry of Tl and its isotopes during magmatic and hydrothermal processes: the peralkaline Ilimaussaq complex, southwest Greenland. Chemical Geology, 366: 1-13

Janney, P. E., Bell, D. R., 2017. Hidden reservoirs in the continental lithosphere? Evidence from Hf-Sr-Nd-Pb isotopes in southern African kimberlite megacrysts. Extended abstracts of the 11th International Kimberlite Conference, Gaborone.

Jones, A. P., Smith, J., Dawson, J. B., 1982. Mantle metasomatism in 14 veined peridotites from Bultfontein Mine, South Africa. Journal of Geology, 90: 435-453

Kennedy, C. S., Kennedy, G. C., 1976. The equilibrium boundary between graphite and diamond. Journal of Geophysical Research, 81(14): 2467-2470

Kiseeva, E. S., Wood, B. J., 2013. A simple model for chalcophile element partitioning between sulphide and silicate liquids with geochemical applications. Earth and Planetary Science Letters, 383: 68-81

Klein, F., Grozeva, N. G., Seewald, J. S., McCollom, T. M., Humphris, S. E., Moskowitz, B., Berquo, T. S., Kahl, W.-A., 2015. Experimental constraints on fluid-rock reactions during incipient serpentinization of harzburgite. American Mineralogist, 100: 991-1002

Konzett, J., Armstrong, R. A., Sweeney, R. J., Compston, W., 1998. The timing of MARID metasomatism in the Kaapvaal mantle: an ion probe study of zircons from MARID xenoliths. Earth and Planetary Science Letters, 160: 133-145

Konzett, J., Krenn, K., Rubatto, D., Hauzenberger, C., Stalder, R., 2014. The formation of saline mantle fluids by open-system crystallization of hydrous silicate-rich vein assemblages – Evidence from fluid inclusions and their host phases in MARID xenoliths from the central Kaapvaal Craton, South Africa. Geochimica et Cosmochimica Acta, 147: 1-25

Konzett, J., Sweeney, R. J., Thompson, A. B., Ulmer, P., 1997. Potassium amphibole stability in the upper mantle: an experimental study in a peralkaline KNCMASH system to 8.5 GPa. Journal of Petrology, 38(5): 537-568

Marty, B., Dauphas, N., 2003. The nitrogen record of crust-mantle interaction and mantle convection from Archean to present. Earth and Planetary Science Letters, 206: 397-410

Mather, K. A., Pearson, D. G., McKenzie, D., Kjarsgaard, B. A., Priestley, K., 2011. Constraints on the depth and thermal history of cratonic lithosphere from peridotite xenoliths, xenocrysts and seismology. Lithos, 125: 729-742

Matson, D. W., Muenow, D. W., Garcia, M. O., 1986. Volatile contents of phlogopite micas from South African kimberlite. Contributions to Mineralogy and Petrology, 93: 399-408

Mattey, D., Lowry, D., Macpherson, C., 1994. Oxygen isotope composition of mantle peridotite. Earth and Planetary Science Letters, 128: 231-241

McDonough, W. F., Sun, S-s., 1995. The composition of the Earth. Chemical Geology, 120: 223-253

McGoldrick, P. J., Keays, R. R., Scott, B. B., 1979. Thallium: A sensitive indicator of rock/seawater interaction and of sulfur saturation of silicate melts. Geochimica et Cosmochimica Acta, 43: 1303-1311

Meyer, H. O., McCallum, M. E., 1986. Mineral inclusions in diamonds from the Sloan kimberlites, Colorado. The Journal of Geology, 94(4): 600-612

Muramatsu, Y., 1983. Geochemical investigations of kimberlites from the Kimberley area, South Africa. Geochemical Journal, 17: 71-86

Nielsen, S. G., Klein, F., Kading, T., Blusztajn, J., Wickham, K., 2015. Thallium as a tracer of fluid-rock interaction in the shallow Mariana forearc. Earth and Planetary Science Letters, 430: 416-426

Nielsen, S. G., Prytulak, J., Blusztajn, J., Shu, Y., Auro, M., Regelous, M., Walker, J., 2017b. Thallium isotopes as tracers of recycled materials in subduction zones: review and new data for lavas from Tonga-Kermadec and Central America. Journal of Volcanology and Geothermal Research, 339: 23-40

Nielsen, S. G., Rehkämper, M., Baker, J., Halliday, A.N., 2004. The precise and accurate determination of thallium isotope compositions and concentrations for water samples by MC-ICPMS. Chemical Geology, 204(1-2): 109-124

Nielsen, S. G., Rehkamper, M., Brandon, A. D., Norman, M. D., Turner, S., O'Reilly, S. Y., 2007. Thallium isotopes in Iceland and Azores lavas – implications for the role of altered crust and mantle geochemistry. Earth and Planetary Science Letters, 264: 332-345

Nielsen, S. G., Rehkamper, M., Halliday, A. N., 2006c. Large thallium isotopic variation in iron meteorites and evidence for lead-205 in the early solar system. Geochimica et Cosmochimica Acta, 70: 2643-2657

Nielsen, S. G., Rehkamper, M., Norman, M. D., Halliday, A. N., Harrison, D., 2006b. Thallium isotopic evidence for ferromanganese sediments in the mantle source of Hawaiian basalts. Nature, 439: 314-317

Nielsen, S. G., Rehkamper, M., Porcelli, D., Andersson, P., Halliday, A. N., Swarzenski, P. W., Latkoczy, C., Gunther, D., 2005. Thallium isotope composition of the upper continental crust and rivers – an investigation of the continental sources of dissolved marine thallium. Geochimica et Cosmochimica Acta, 19(8): 2007-2019

Nielsen, S. G., Rehkamper, M., Prytulak, J., 2017a. Investigation and application of thallium isotope fractionation. Reviews in Mineralogy and Geochemistry, 82: 759-798

Nielsen, S. G., Rehkamper, M., Teagle, D. A. H., Butterfield, D. A., Alt, J. C., Halliday, A. N., 2006a. Hydrothermal fluid fluxes calculated from the isotopic mass balance of thallium in the ocean crust. Earth and Planetary Science Letters, 251(1-2): 120-133

Nielsen, S. G., Shimizu, N., Lee, C.-T. A., Behn, M. D., 2014. Chalcophile behaviour of thallium during MORB melting and implications for the sulfur content of the mantle Geochemistry, Geophysics, Geosystems, 15: 4905-4919

Nielsen, S. G., Williams, H. M., Griffin, W. L., O'Reilly, S. Y., Pearson, N., Viljoen, F., 2009. Thallium isotopes as a potential tracer for the origin of cratonic eclogites. Geochimica et Cosmochimica Acta, 73(24): 7387-7398

Nielsen, S. G., Yogodzinski, G., Prytulak, J., Plank, T., Kay, S. M., Kay, R. W., Blusztajn, J., Owens, J. D., Auro, M., Kading, T., 2016. Tracking along-arc sediment inputs to the Aleutian arc using thallium isotopes. Geochimica et Cosmochimica Acta, 181: 217-237

Noll, P. D., Newsom, H. E., Leeman, W. P., Ryan, J. G., 1996. The role of hydrothermal fluids in the production of subduction zone magmas: Evidence from siderophile and chalcophile trace elements and boron. Geochimica et Cosmochimica Acta, 60(4): 587-611

O'Reilly, S. Y., Griffin, W. L., 2006. Imaging global chemical and thermal heterogeneity in the subcontinental lithospheric mantle with garnets and xenoliths: geophysical implications. Tectonophysics, 416: 289-309

Pearson, D. G., Rogers, N. W., Irving, A. J., Smith, C. B., Hawkesworth, C. J., 1995. Source regions of kimberlites and lamproites: constraints from Re-Os isotopes. Extended abstracts of the 6th International Kimberlite Conference, Novosibirsk

Peterson, T. D., LeCheminant, A. N., 1993. Glimmerite xenoliths in early Proterozoic ultrapotassic rocks from the Churchill Province. The Canadian Mineralogist, 31: 801-819

Phillips, D., Harris, J. W., Viljoen, K. S., 2004. Mineral chemistry and thermobarometry of inclusions from De Beers pool diamonds, Kimberley, South Africa. Lithos, 77: 155-179

Prytulak, J., Brett, A., Webb, M., Plank T., Rehkamper, M., Savage, P. S., Woodhead, J., 2017. Thallium elemental behaviour and stable isotope fractionation during magmatic processes. Chemical Geology, 448: 71-83

Prytulak, J., Nielsen, S. G., Plank, T., Barker, M., Elliott, T., 2013. Assessing the utility of thallium and thallium isotopes for tracing subduction zone inputs to the Mariana arc. Chemical Geology, 345: 139-149

Rader, S. T., Mazdab, F. K., Barton, M. D., 2018. Mineralogical thallium geochemistry and isotope variations from igneous, metamorphic, and metasomatic systems. Geochimica et Cosmochimica Acta, 243: 42-65

Rehfeldt, T., Foley, S. F., Jacob, D. E., Carlson, R. W., Lowry, D., 2008. Contrasting types of metasomatism in dunite, wehrlite and websterite xenoliths from Kimberley, South Africa. Geochimica et Cosmochimica Acta, 72(23): 5722-5756

Rehkamper, M., Halliday, A. N., 1999. The precise measurement of Tl isotopic compositions by MC-ICP-MS: application to the analysis of geological materials and meteorites. Geochimica et Cosmochimica Acta, 63(6): 935-944

Rehkämper, M., Frank, M., Hein, J. R., Halliday, A., 2004. Cenozoic marine geochemistry of thallium deduced from isotopic studies of ferromanganese crusts and pelagic sediments. Earth and Planetary Science Letters, 219(1-2): 77-91

Rehkamper, M., Frank, M., Hein, J. R., Porcelli, D., Halliday, A., Ingri, J., Liebetrau, V., 2002. Thallium isotope variations in seawater and hydrogenetic, diagenetic, and hydrothermal ferromanganese deposits. Earth and Planetary Science Letters, 197: 65-81

Rudnick, R. L., Gao, S., 2014. Composition of the continental crust. In: Treatise on Geochemistry, Volume 3. Rudnick, R. L. (ed.), p. 1-64

Salters, V. J. M., Stracke, A., 2004. Composition of the depleted mantle. Geochemistry Geophysics Geosystems, 5(5)

Shaw, D. M., 1952. The geochemistry of thallium. Geochimica et Cosmochimica Acta, 2: 118-154

Shu, Y., Nielsen, S. G., Zeng, Z., Shinjo, R., Blusztajn, J., Wang, X., Chen, S., 2017. Tracing subducted sediment inputs to the Ryukyu arc-Okinawa trough system: evidence from thallium isotopes. Geochimica et Cosmochimica Acta, 217:462-491

Shu, Y., Nielsen, S. G., Marschall, H. R., John, T., Blusztajn, J., Auro, M., 2019. Closing the loop: subducted eclogites match thallium isotope compositions of ocean island basalts. Geochimica et Cosmochimica Acta, 250: 130-148

Smith, C. B., 1983. Pb, Sr and Nd isotopic evidence for sources of southern African Cretaceous kimberlites. Nature, 304: 51-54

Smith, C. B., Allsopp, H., Kramers, J., Hutchinson, G., Roddick, J., 1985. Emplacement ages of Jurassic-Cretaceous South African kimberlites by the Rb-Sr method on

phlogopite and whole-rock samples. South African Journal of Geology, 88(2): 249-266

Soltys, A., Giuliani, A., Phillips, D., 2018. A new approach to reconstructing the composition and evolution of kimberlite melts: a case study of the archetypal Bultfontein kimberlite (Kimberley, South Africa). Lithos, 304-307: 1-15

Soltys, A., Giuliani, A., Phillips, D., Kamenetsky, V. S., Maas, R., Woodhead, J., Rodemann, T., 2016. In-situ assimilation of mantle minerals by kimberlitic magmas – direct evidence from a garnet wehrlite xenolith entrained in the Bultfontein kimberlite (Kimberley, South Africa). Lithos, 256-257: 182-196

Stamm, N., Schmidt, M. W., 2017. Asthenospheric kimberlites: volatile contents and bulk compositions at 7 GPa. Earth and Planetary Science Letters, 474: 309-321

Sweeney, R. J., Thompson, A. B., Ulmer, P., 1993. Phase relations of a natural MARID composition and implications for MARID genesis, lithospheric melting and mantle metasomatism. Contributions to Mineralogy and Petrology, 115: 225-241

van Achterbergh, E., Griffin, W. L., Stiefenhofer, J., 2001. Metasomatism in mantle xenoliths from the Letlhakane kimberlites: estimation of element fluxes. Contributions to Mineralogy and Petrology, 141: 397-414

Vink, B. W., 1993. The behaviour of thallium in the (sub) surface environment in terms of Eh and pH. Chemical Geology, 109: 119-123

Walter, M. J., 1998. Melting of garnet peridotite and the origin of komatiite and depleted lithosphere. Journal of Petrology, 39(1): 29-60

Wang, Y., Foley, S. F., Prelevic, D., 2017. Potassium-rich magmatism from a phlogopite-free source. Geology, 45(5): 467-470

Wang, Z., Lazarov, M., Steinmann, L. K., Becker, H., Zou, Z., Geng, X., 2018. The distribution of lead and thallium in mantle rocks: insights from the Balmuccia peridotite massif (Italian Alps). American Mineralogist, 103: 1185-1199

Waters, F. G., 1987. A suggested origin of MARID xenoliths in kimberlites by high pressure crystallization of an ultrapotassic rock such as lamproite. Contributions to Mineralogy and Petrology, 95(4): 523-533

Weiss, Y., Class, C., Goldstein, S. L., Hanyu, T., 2016. Key new pieces of the HIMU puzzle from olivines and diamond inclusions. Nature, 537: 666

Winterburn, P. A., Harte, B., Gurney, J. J., 1990. Peridotite xenoliths from the Jagersfontein kimberlite pipe: I. Primary and primary-metasomatic mineralogy. Geochimica et Cosmochimica Acta, 54: 329-341

Woodhead, J., Hergt, J., Phillips, D., Paton, C., 2009. African kimberlites revisited: in situ Sr-isotope analysis of groundmass perovskite. Lithos, 112S: 311-317

Zhang, H.-F., Mattey, D. P., Grassineau, N., Lowry, D., Brownless, M., Gurney, J. J., Menzies, M. A., 2000. Recent fluid processes in the Kaapvaal craton, South Africa: coupled oxygen isotope and trace element disequilibrium in polymict peridotites. Earth and Planetary Science Letters, 176(1): 57-72

Zhang, H.-F., Menzies, M. A., Mattey, D. P., Hinton, R. W., Gurney, J. J., 2001. Petrology, mineralogy and geochemistry of oxide minerals in polymict xenoliths from the Bultfontein kimberlites, South Africa: implication for low bulk-rock oxygen isotopic ratios. Contributions to Mineralogy and Petrology, 141: 367-379

Zindler, A., Jagoutz, E., Goldstein, S., 1982. Nd, Sr and Pb isotopic systematics in a three-component mantle: a new perspective. Nature, 298: 519-523

Figure Captions

Figure 1: Summary graph plotting Tl content in MARID and PIC mica samples used in this study (Fitzpayne et al., 2018a), compared to phyllosilicates and sulfides analysed by Rader et al. (2018), sulfides in lherzolites (Nielsen et al., 2014), and a harzburgite whole-rock analysis from the Eifel volcanic field (Germany; Nielsen et al., 2015); grey field delineates range of Tl content in the continental crust (0.5-1.6 µg/g; Rudnick and Gao, 2014)

Figure 2: Map of southern Africa, modified after le Roex and Class (2016), showing extent of Kaapvaal craton (grey) and surrounding fold belts (delineated by dashed lines); localities from which samples for this study were derived are the Kimberley kimberlites (filled triangle) and the Newlands orangeite (open triangle)

Figure 3: Photomicrographs of: (a) MARID sample WES-2 (Wesselton) in plane-polarised light (PPL), containing clinopyroxene (centre) and phlogopite, which displays extensive zonation, based on both colour and texture; greenish-coloured kimberlitic material has infiltrated along grain boundaries; (b) MARID sample AJE-2422 (Bultfontein) in PPL, containing K-richterite (amphibole), ilmenite, and unzoned phlogopite; (c) PPL (left) and cross-polarised light (XPL, right) photomicrographs of PIC sample AJE-541 (Kamfersdam), which contains clinopyroxene (not shown) and phlogopite. Phlogopite in this sample (and other PIC samples) displays kink-banding (visible in PPL) as well as a bimodal grainsize distribution (more easily recognised in XPL); and (d) PIC sample FW-20 (Bultfontein) in PPL, which contains sub-rounded to

rounded clinopyroxene porphyroclasts, set amongst a groundmass of predominantly fine-grained phlogopite

Figure 4: Thallium contents (µg/g) in MARID and PIC phlogopite bulk mineral separates calculated by matching beam-size intensities during solution MC-ICP-MS (this study) vs average thallium contents (µg/g) in MARID and PIC phlogopite cores analysed *in situ* (data from Fitzpayne et al., 2018a); analyses of standard reference materials (BCR-2, Mica-Mg, and Mica-Fe) also plotted, with preferred values (data from Brett et al., 2018, and references therein) along x-axis; error bars represent external 2 s.d. for solution-mode MC-ICP-MS measurements, which are relatively large compared to uncertainties by LA-ICP-MS; 1:1 line plotted for reference

Figure 5: Tl (µg/g) vs (a) Al_2O_3 (wt.%); (b) Mg# (100*Mg/(Mg+Fe)); (c) K_2O (wt.%); and (d) Rb (µg/g) abundances from *in situ* electron microprobe and laser ablation ICP-MS phlogopite core analyses from Fitzpayne et al. (2018a); symbols as in Fig. 4

Figure 6: Tl (µg/g; *in situ* analyses of cores; Fitzpayne et al., 2018a) vs $\varepsilon^{205}Tl$ in MARID and PIC phlogopite samples from this study (symbols as in Fig. 4), compared to biotite and phlogopite separates analysed by Rader et al. (2018; white circles); grey field shows the expected mantle $\varepsilon^{205}Tl$ value (-2 ± 1; Nielsen et al., 2006a, 2017a); error bars shown for three samples denote external 2 s.d. of multiple analyses; for all other samples, internal 2 s.d. is considered to be the same as the value for the Aldrich solution standard (± 0.5), and is approximately the same as symbol size

Figure 7: Graph of Tl content (μg/g) vs ε^{205}Tl showing mixing lines (thin black lines) between the primitive mantle (0.0035 μg/g Tl; ε^{205}Tl = –2) and continental crust, low temperature-altered oceanic crust (low-T AOC), pelagic clays, and Fe-Mn sediments (white boxes; see text for explanation; data from Nielsen et al., 2017a; Prytulak et al., 2013, and references therein). Dashed lines denote 1% mixing of crustal components to the primitive mantle composition. Mantle ε^{205}Tl range (grey box), and kimberlite melt source composition (for Tl content, see text; ε^{205}Tl range as for PIC in Table 2) shown for comparison; red box denotes range in Tl content in primitive (i.e., undepleted) mantle (0.0035 μg/g: McDonough and Sun, 1995), depleted mantle (0.00035 μg/g: Salters and Stracke, 2004) and a harzburgite bulk-rock analysis (0.00105 μg/g: Nielsen et al., 2015)

Figure 8: Graph of Tl content (μg/g) vs ε^{205}Tl showing two-step mass balance mixing models: first step demonstrates mixing between continental crust composition and ranges for low temperature-altered oceanic crust (low-T AOC), pelagic clays, and Fe-Mn sediments (white boxes; see text for explanation); dotted line denotes Tl-ε^{205}Tl compositions created by 55% addition of low temperature-AOC to 45% continental crust; MARID phlogopite (blue circles, this study) plotted for comparison. Grey box denotes mantle ε^{205}Tl range; red box shows composition of MARID parental melt source, based on MARID phlogopite ε^{205}Tl values and partition coefficient constraints (see text). Second mixing step (dashed lines) plotted for mixtures of primitive mantle (or high temperature-AOC) and continental crust (500 μg/g, ε^{205}Tl = -1.5) or 55-45 mix of low temperature-AOC/continental crust (800 μg/g, ε^{205}Tl = -3.9); black circles denote the compositions that result from, respectively, 50% and 31% incorporation of these recycled components to the primitive mantle composition

Figure 9: (a) photomicrograph of sample FW-20 containing ilmenite (ilm) and clinopyroxene (cpx), which is being replaced by brown-coloured rinds composed of serpentine- and talc-group minerals; larger phlogopite (phl) porphyroclasts are separated by fine-grained, sheared phlogopite and carbonate; (b) back-scattered electron image of chromatite (chr: $CaCrO_4$) inclusion in a clinopyroxene (cpx) porphyroclast in sample FW-20; composition of inclusion varies within and between grains (see Supplementary Table 2)

Supplementary Figure 1: Phlogopite $\varepsilon^{205}Tl$ values from this study vs (a) Al_2O_3 (wt.%); (b) Mg#; and (c) K_2O (wt.%) abundances from *in situ* electron probe microanalysis of phlogopite cores (Fitzpayne et al., 2018a); panel (b) is an inset of the overall $\varepsilon^{205}Tl$-Mg# variation found in the study of Rader et al. (2018; white circles); dashed lines represent the reported mantle $\varepsilon^{205}Tl$ value (-2 ± 1; Nielsen et al., 2006a, 2017a); symbols as in Fig. 7

Supplementary Figure 2: Phlogopite $\varepsilon^{205}Tl$ values from this study vs (a) $^{87}Sr/^{86}Sr_i$; (b) εNd_i; (c) εHf_i; and (d) $^{206}Pb/^{204}Pb_i$ values in coexisting clinopyroxene and amphibole (Fitzpayne et al., 2019); symbols as in Fig. 7

Supplementary Figure 3: Tl content (µg/g) vs Tl content (µg/g) for *in situ* analyses of MARID phlogopite rims (data from Fitzpayne et al., 2018b) compared to their respective cores (data from Fitzpayne et al., 2018a); 1:1 line plotted for reference

Figure 1
Click here to download high resolution image

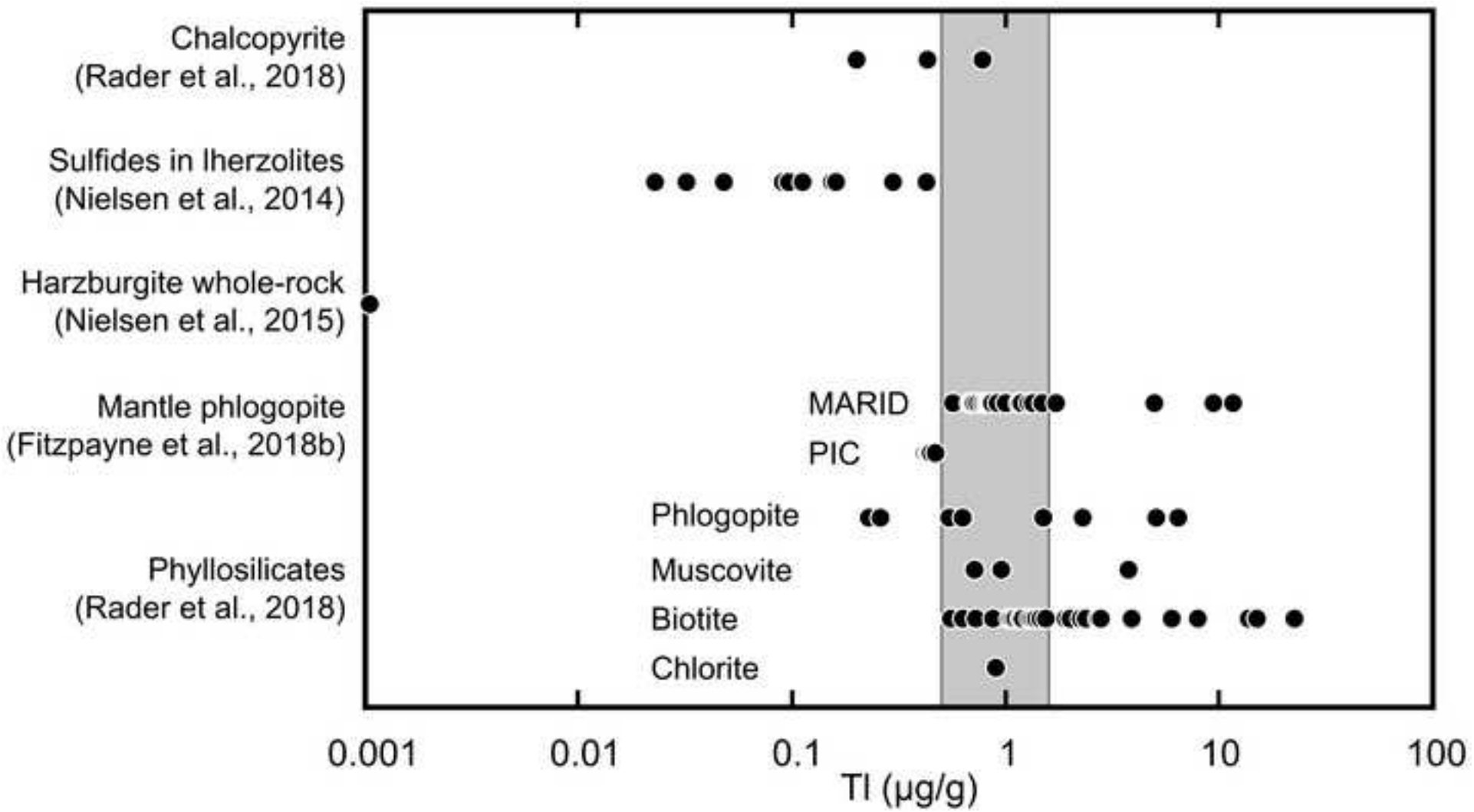

Figure 2
Click here to download high resolution image

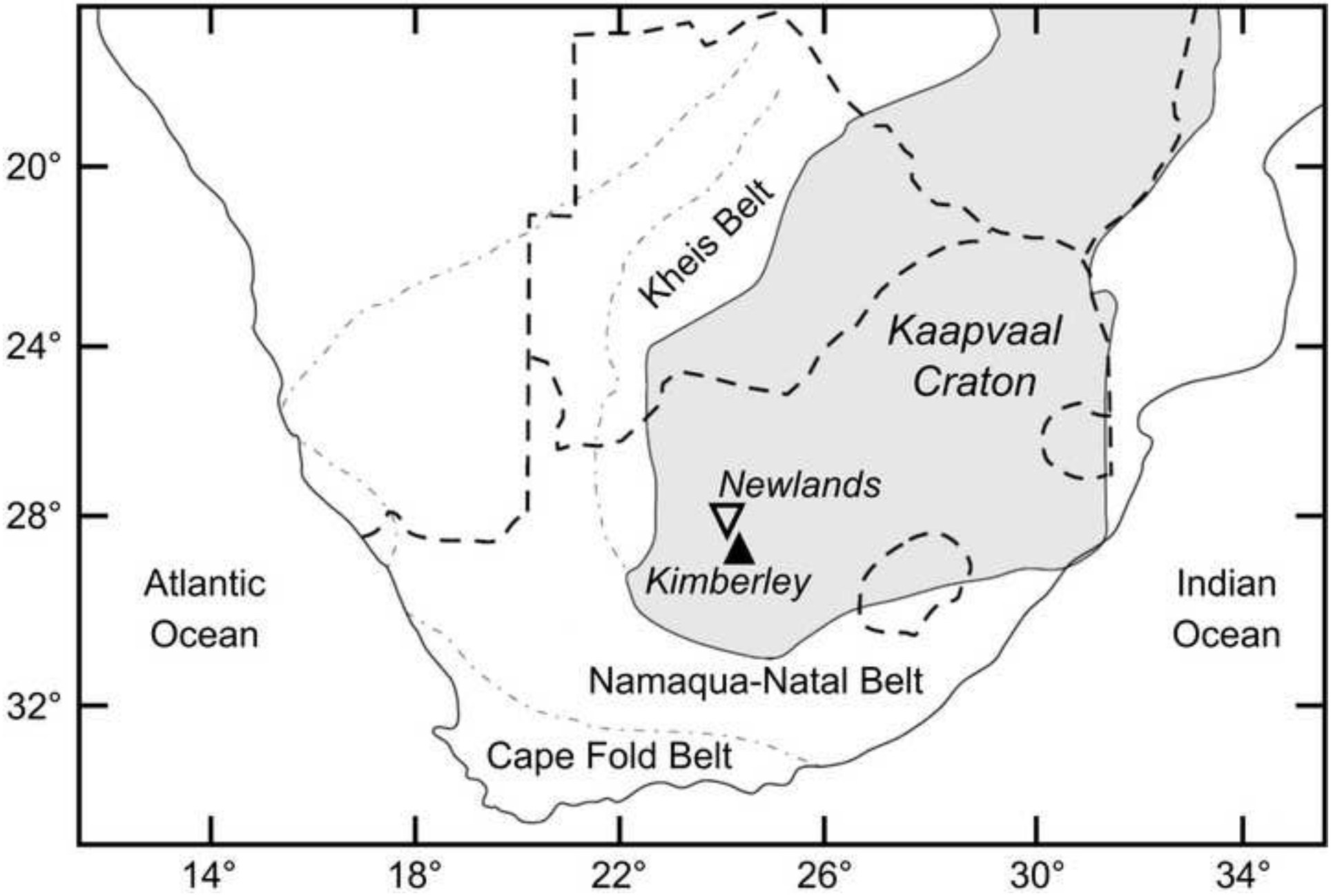

Figure 3

Click here to download high resolution image

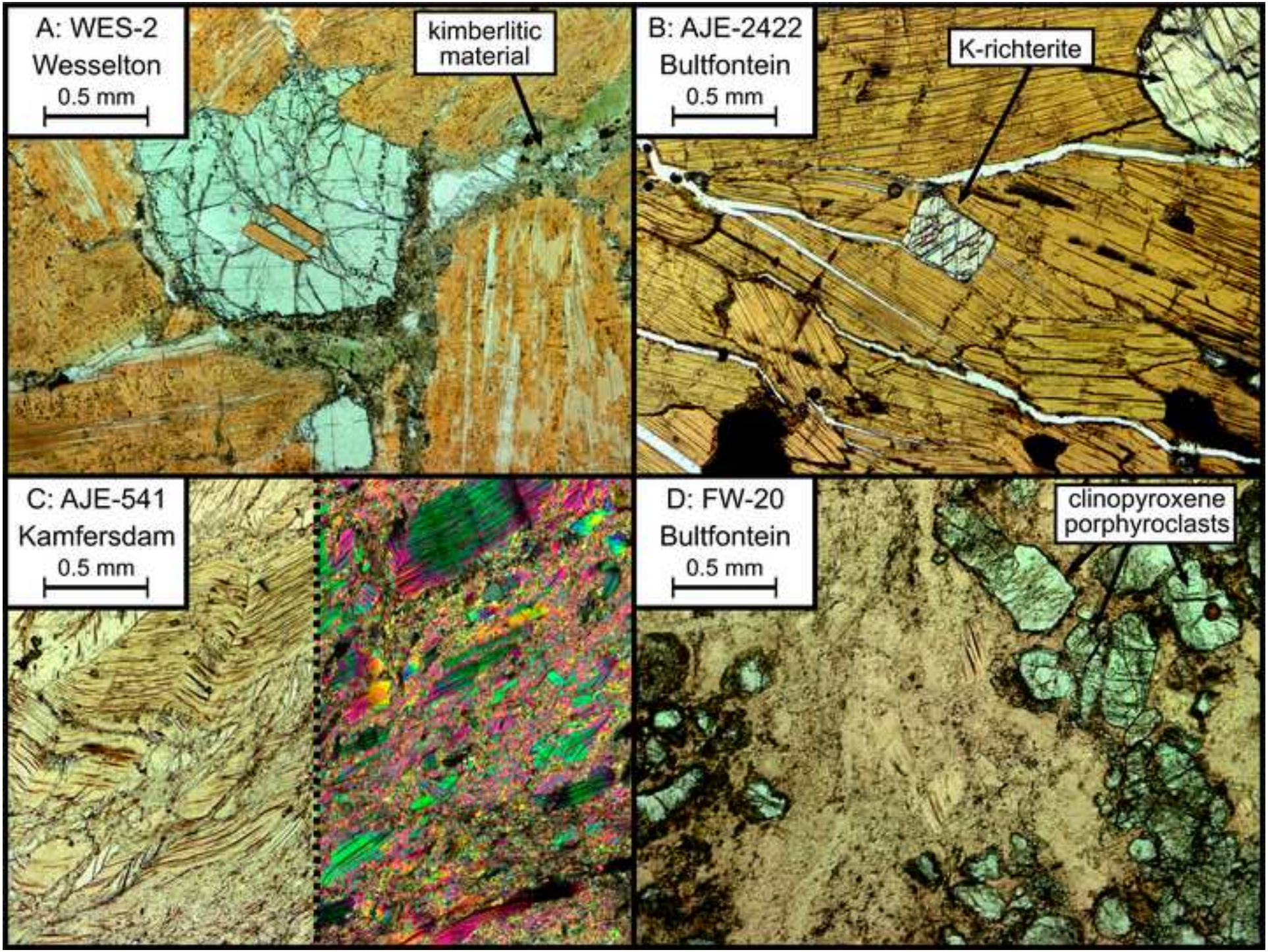

Figure 4
Click here to download high resolution image

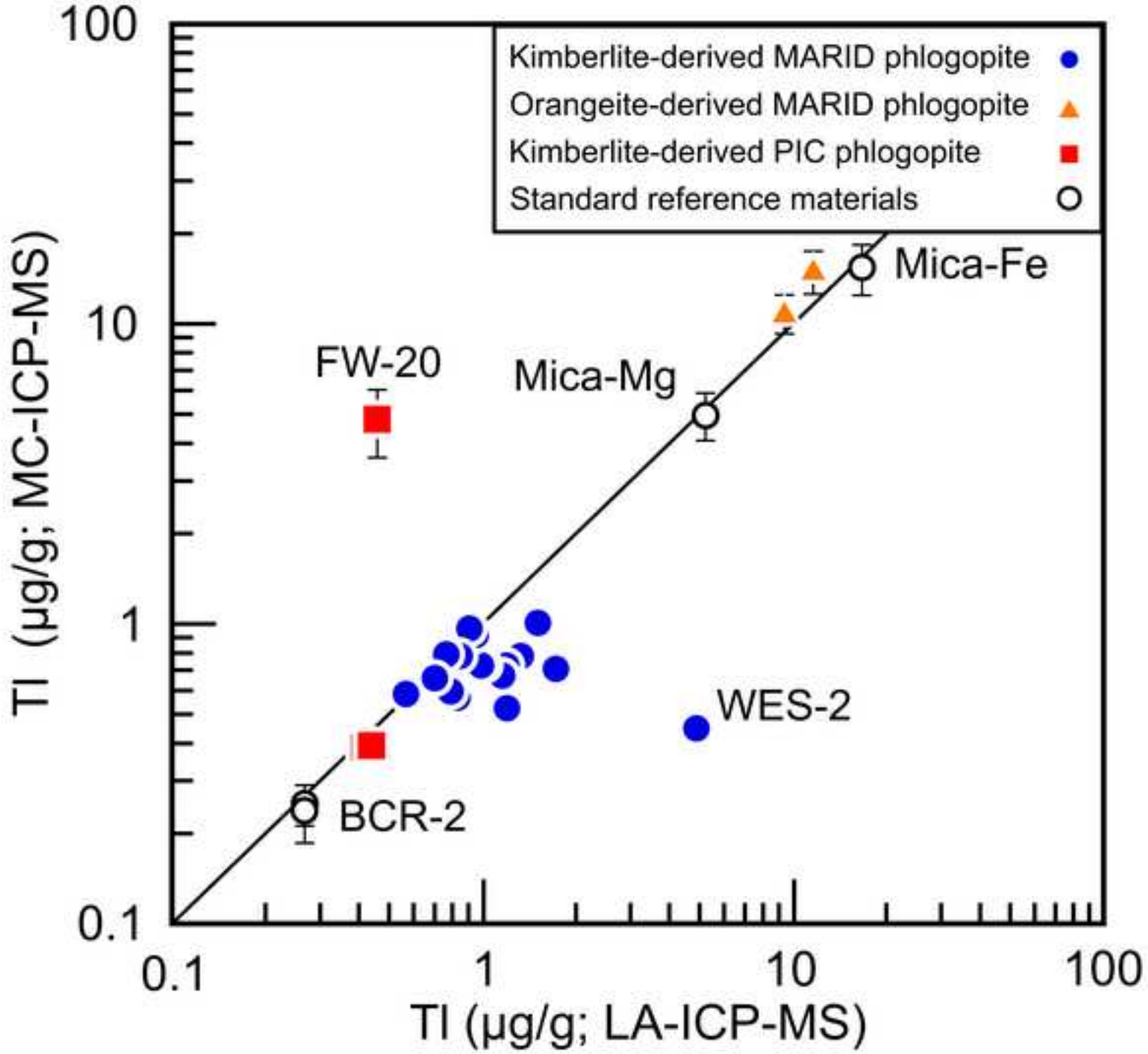

Figure 5

Click here to download high resolution image

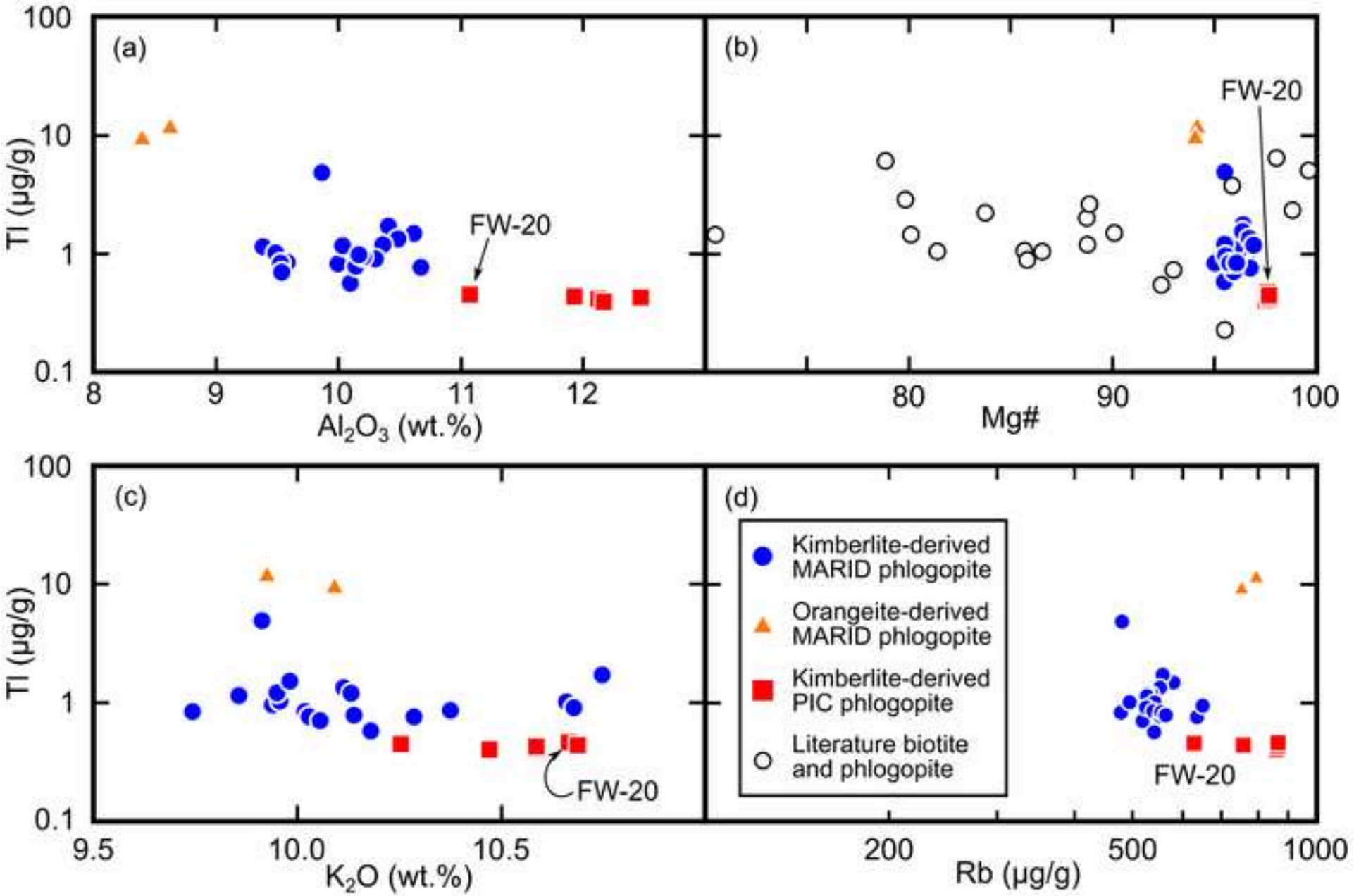

Figure 6
Click here to download high resolution image

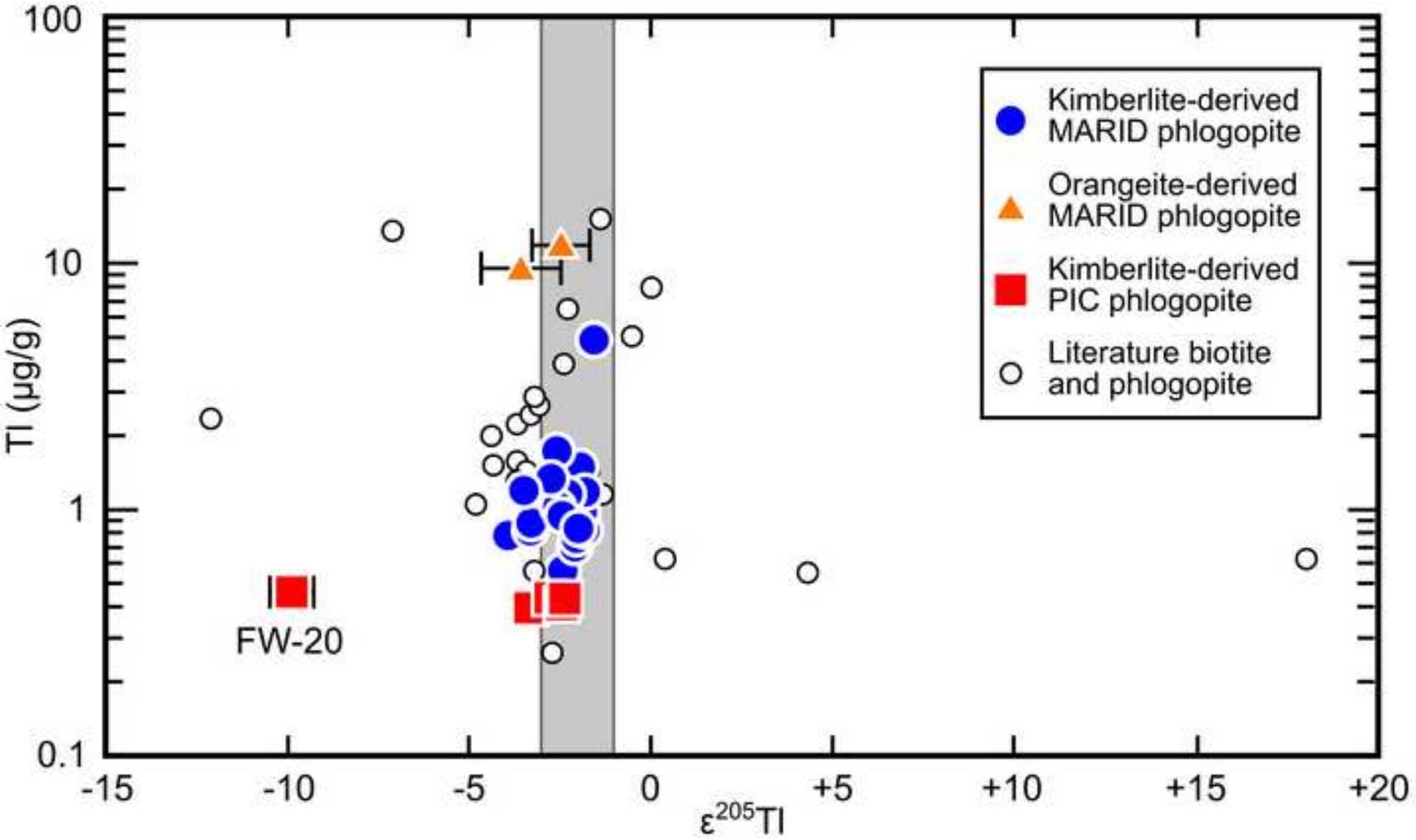

Figure 7

Click here to download high resolution image

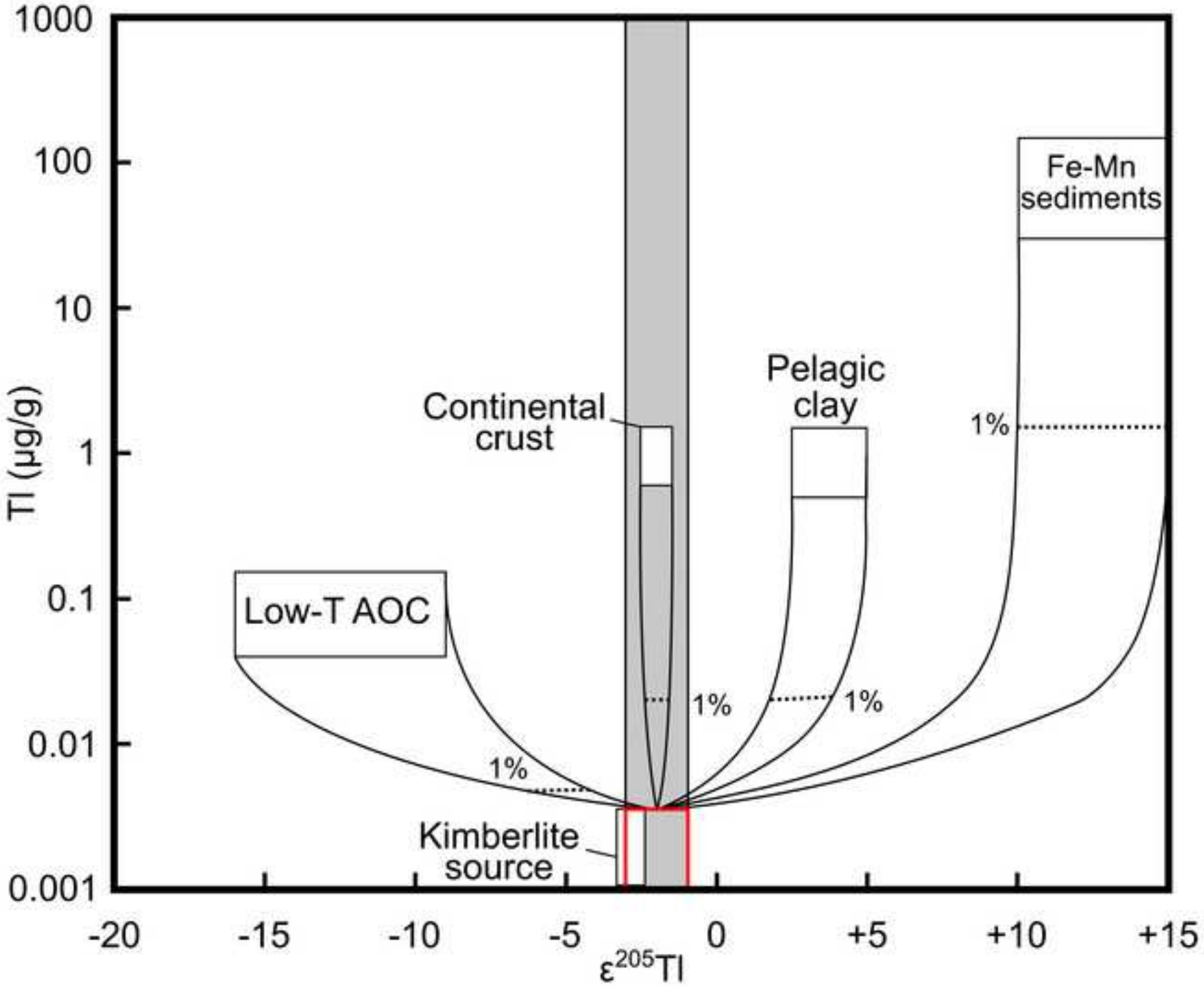

Figure 8

Click here to download high resolution image

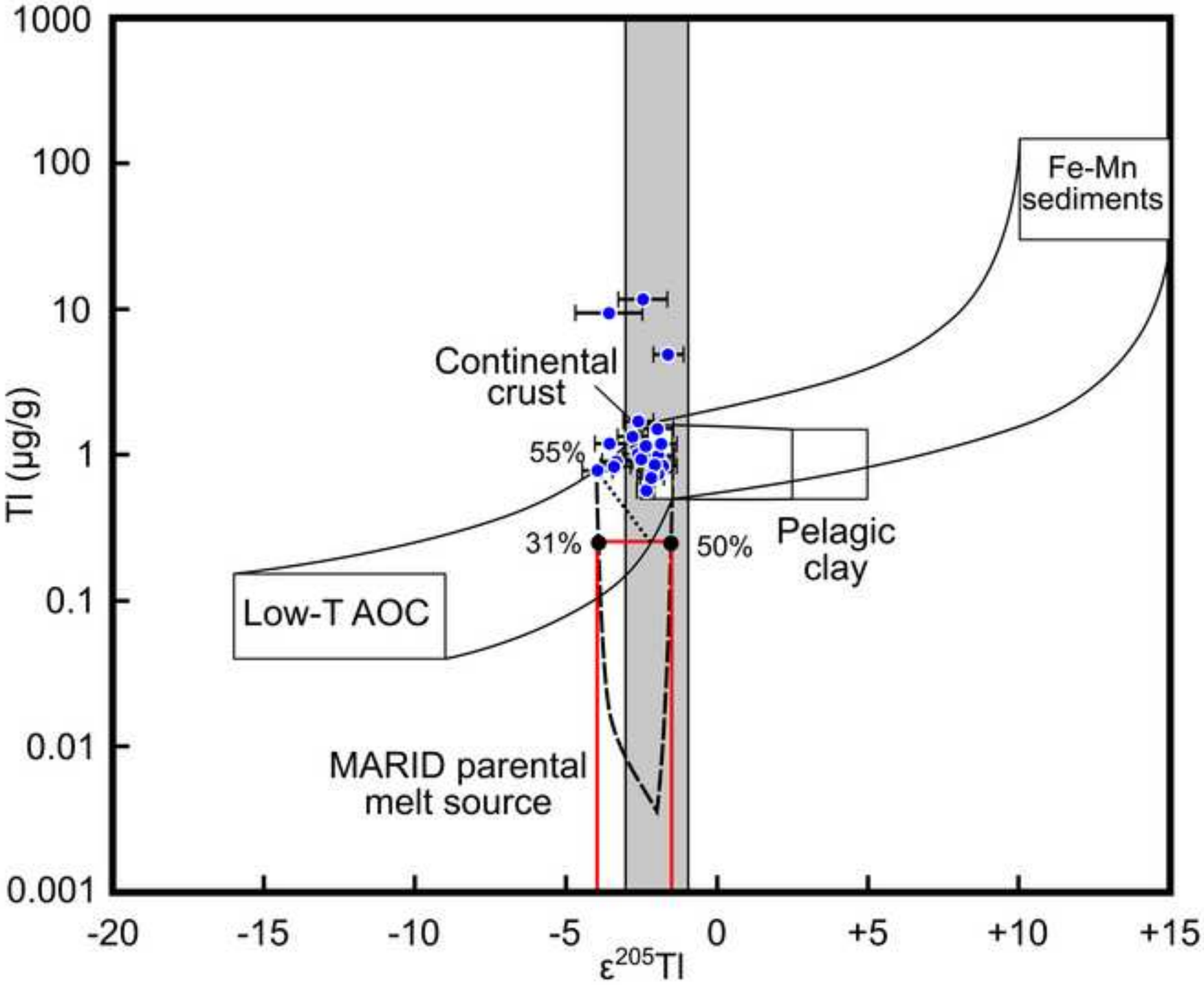

Figure 9

Click here to download high resolution image

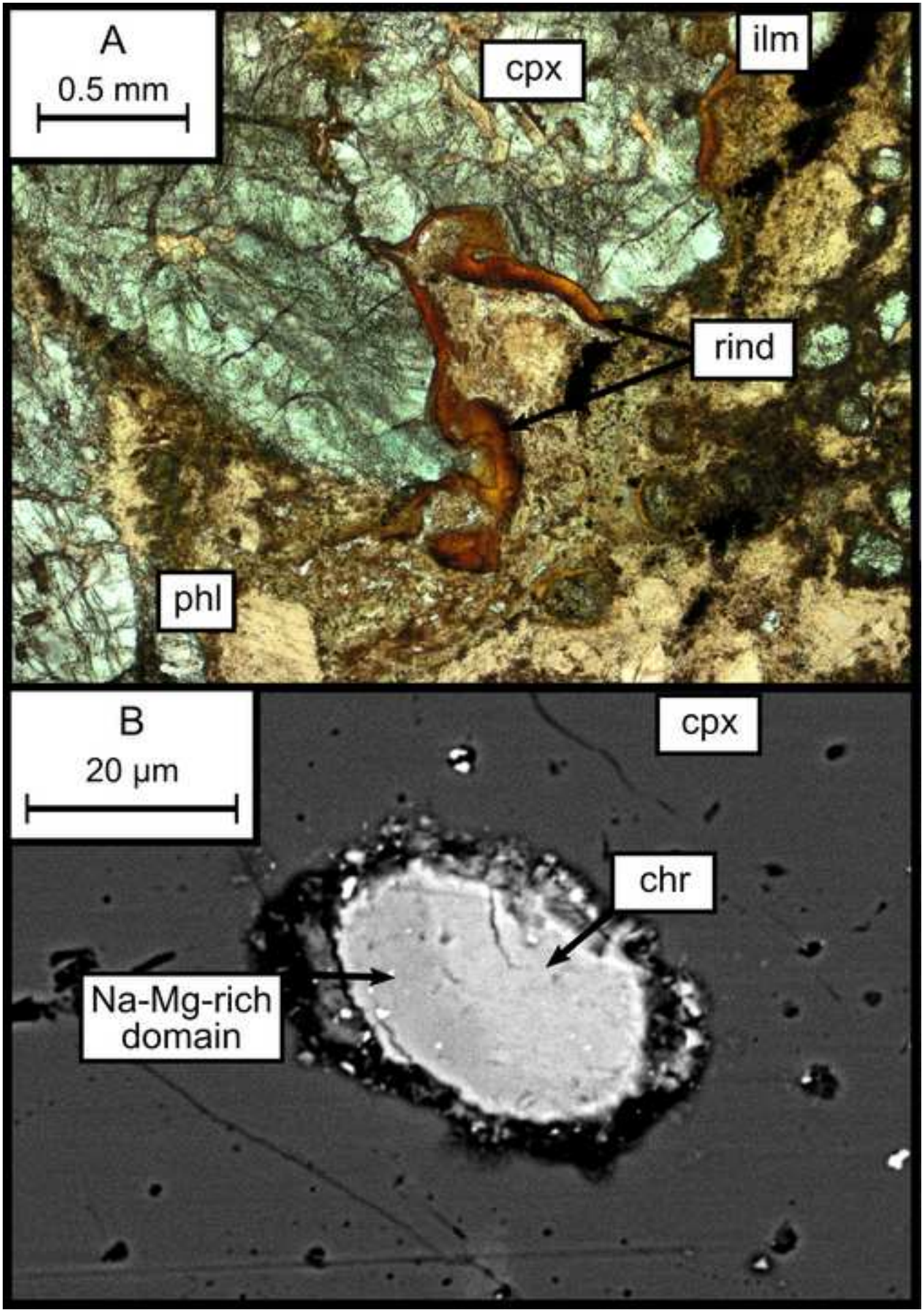

Supplementary Figure 1

Click here to download high resolution image

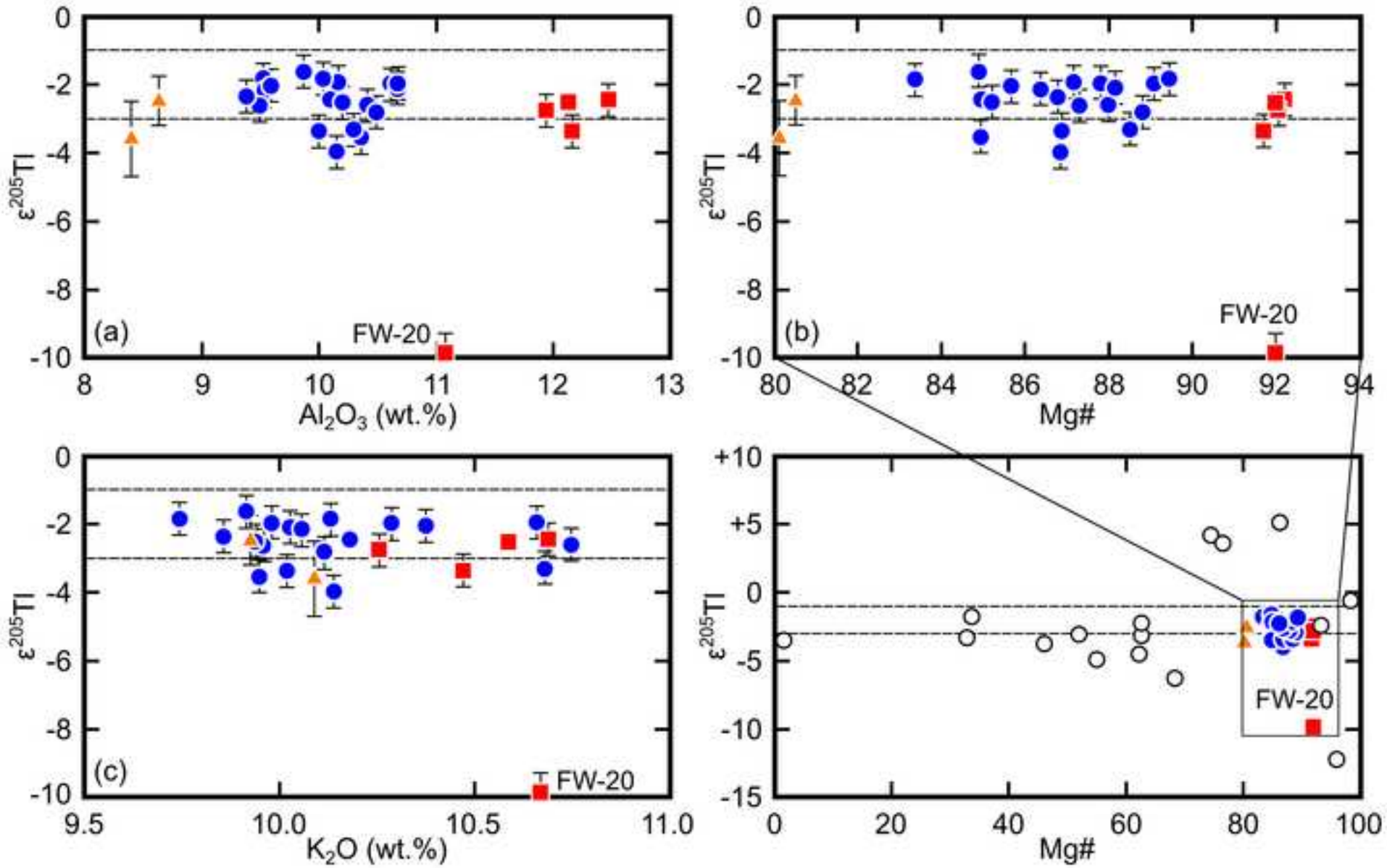

Supplementary Figure 2

Click here to download high resolution image

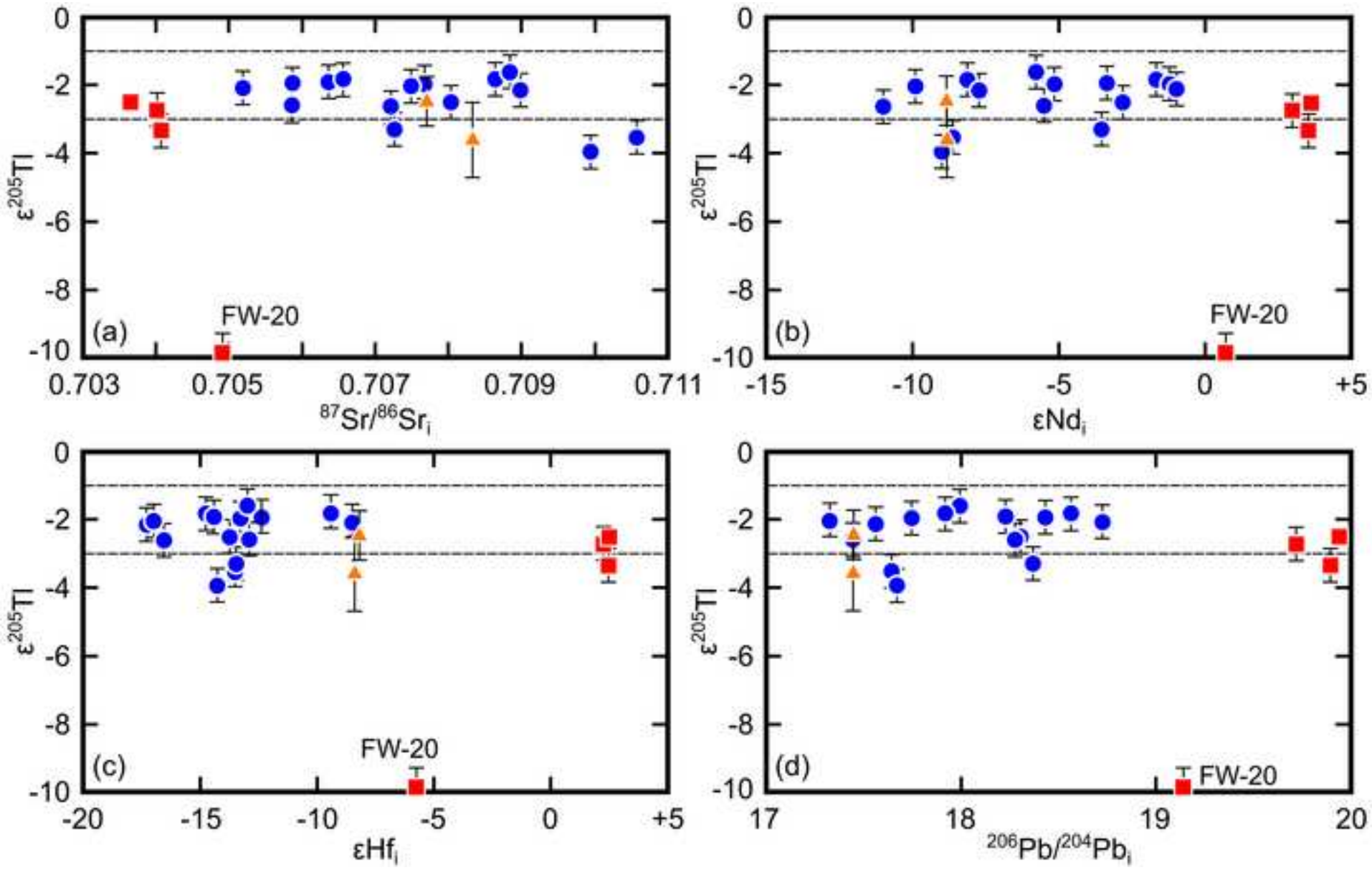

Supplementary Figure 3

Click here to download high resolution image

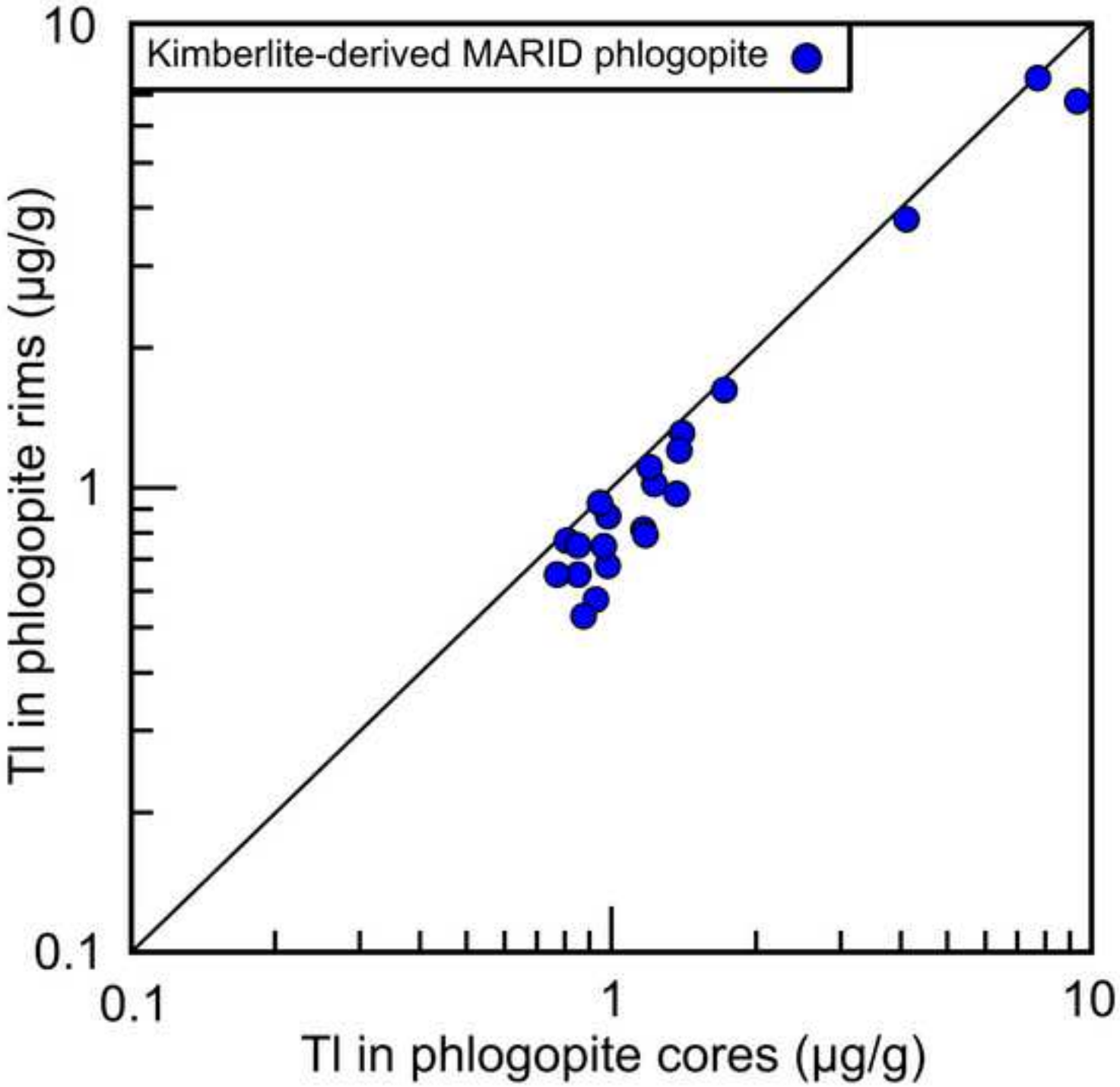

Table 1
Click here to download Table: Table 1.docx

Table 1: Petrographic and *in situ* geochemical data for MARID and PIC samples in this study

					w/r [a]	Phlogopite [b]			
Sample type	Sample name	Locality [c]	Latitude (S)/ Longitude (E)	Texture	Tl (µg/g)	Tl (µg/g)	Al_2O_3 (wt.%)	K_2O (wt.%)	Mg#
MARID	AJE-2333	BLF	28°46'/24°47'	Foliated	0.52	0.77	10.7	10.0	88.2
	AJE-2334	BLF	28°46'/24°47'	Foliated	0.33	0.76	10.7	10.3	89.1
	AJE-2335	BLF	28°46'/24°47'	Foliated	0.44	0.95	10.2	9.9	85.2
	AJE-2422	BLF	28°46'/24°47'	Granular	0.72	0.85	9.6	10.4	85.6
	AJE-319	DeB	28°44'/24°47'	Granular	0.90	1.19	10.0	10.1	89.4
	AJE-326	KIM	28°45'/24°45'	Granular	0.25	0.91	10.3	10.7	88.5
	AJE-333	DeB	28°44'/24°47'	Foliated	0.75	1.03	9.5	10.0	87.3
	AJE-335	DeB	28°44'/24°47'	Foliated	0.66	0.84	9.5	9.7	83.4
	AJE-360	BLF	28°46'/24°47'	Granular	1.25	1.33	10.5	10.1	88.8
	AJE-537	KAM	28°42'/24°44'	Granular	1.06	1.20	10.4	10.0	84.9
	AJE-559	KAM	28°42'/24°44'	Granular	0.57	0.57	10.1	10.2	85.0
	BLFX-26	BLF	28°46'/24°47'	Foliated	0.29	0.70	9.5	10.1	86.4
	JJG-2040	BLF	28°46'/24°47'	Granular	0.60	0.79	10.1	10.1	86.8
	JJG-2315	BLF	28°46'/24°47'	Foliated	1.33	1.51	10.6	10.0	87.8
	JJG-2326	BLF	28°46'/24°47'	Granular	0.89	1.00	10.2	10.7	87.2
	JJG-2331	BLF	28°46'/24°47'	Granular	1.53	1.72	10.4	10.7	88.0
	KFDX-3	KAM	28°42'/24°44'	Granular	1.13	1.15	9.4	9.9	86.8
	KPX-1	KIM	28°45'/24°45'	Granular	0.83	0.84	10.0	10.0	86.9
	WES-2	WES	28°46'/24°50'	Granular	3.48	4.89	9.9	9.9	84.9
	AJE-67	NEW	28°20'/24°02'	Foliated	2.15	11.64	8.6	9.9	80.5
	AJE-69	NEW	28°20'/24°02'	Foliated	1.57	9.40	8.4	10.1	80.1
PIC	AJE-540	KAM	28°42'/24°44'	Foliated		*bd* [d]	12.2	10.5	91.7
	AJE-541	KAM	28°42'/24°44'	Foliated	0.42	0.43	12.5	10.7	92.2
	AJE-568	KAM	28°42'/24°44'	Foliated	0.40	0.44	11.9	10.3	92.0
	JJG-2327	BLF	28°46'/24°47'	Foliated	0.38	0.42	12.1	10.6	92.0
	FW-20	BLF	28°46'/24°47'	Porphyroclastic	0.35	0.46	11.1	10.7	92.0

[a] Reconstructed whole-rock Tl abundance from Fitzpayne et al. (2018a)

[b] In situ geochemical data from Fitzpayne et al. (2018a)
[c] BLF = Bultfontein; DeB = De Beers; KAM = Kamfersdam; KIM = Kimberley; NEW = Newlands; WES = Wesselton
[d] *In situ* Tl concentration in sample AJE-540 was bd (below detection) in data from Fitzpayne et al. (2018a); however, sample included in this study based on observation that PIC samples display generally uniform compositions

Table 2: Thallium contents and isotopic compositions of MARID and PIC phlogopite separates measured by MC-ICP-MS in this study

Sample type	Sample	n [a]	Tl (µg/g)	ε^{205}Tl	2 s.d. [b]
Kimberlite-derived MARID	AJE-2333	1	0.78	-2.1	*0.5*
	AJE-2334	1	0.79	-1.9	*0.5*
	AJE-2335	1	0.91	-2.5	*0.5*
	AJE-2422	1	0.78	-2.0	*0.5*
	AJE-319	1	0.72	-1.8	*0.5*
	AJE-326	1	0.97	-3.3	*0.5*
	AJE-333	1	0.73	-2.6	*0.5*
	AJE-335	1	0.57	-1.8	*0.5*
	AJE-360	1	0.78	-2.8	*0.5*
	AJE-537	1	0.52	-3.5	*0.5*
	AJE-559	2	0.58	-2.3	0.3
	BLFX-26	1	0.66	-2.1	*0.5*
	JJG-2040	1	0.59	-3.9	*0.5*
	JJG-2315	1	1.00	-2.0	*0.5*
	JJG-2326	1	0.73	-1.9	*0.5*
	JJG-2331	1	0.71	-2.6	*0.5*
	KFDX-3	1	0.67	-2.3	*0.5*
	KPX-1	1	0.56	-3.4	*0.5*
	WES-2	1	0.45	-1.6	*0.5*
Orangeite-derived MARID	AJE-67	4	15.13	-2.4	0.8
	AJE-69	5	10.91	-3.6	1.1
Kimberlite-derived PIC	AJE-540	1	0.38	-3.3	*0.5*
	AJE-541	1	0.39	-2.4	*0.5*
	AJE-568	1	0.39	-2.7	*0.5*
	JJG-2327	2	0.38	-2.5	0.1
	FW-20	3	4.85	-9.9	0.6

[a] Number of measurements

[b] 2 s.d. here represents external reproducibility of multiple measurements; numbers in *italics* indicate the sample has been ascribed a 2 s.d. of 0.5 epsilon units (Nielsen et al., 2017a)

Supplementary Table 1

Click here to download Table: Supplementary Table 1.docx

Supplementary Table 1: Thallium isotopic compositions of standard reference materials

Reference materials	Tl (µg/g)	2 s.d.	ε^{205}Tl	2 s.d.	# digestions	# measurements
BCR-2	244	46	-2.4	0.8	2	7
Accepted value [a]	*267*		*-2.4*	*0.2*		
Mica-Mg	5027	897	-0.2	0.5	1	4
Accepted value	*5270*		*-0.1*	*0.9*		
Mica-Fe	15560	2986	-3.1	0.9	1	5
Accepted value	*16800*		*-3.4*	*0.7*		
Aldrich			-1.0	0.3	n/a	11
Accepted value			*-0.8*	*0.3*		

[a] All accepted values from Brett et al. (2018), and references therein

Supplementary Table 2
Click here to download Table: Supplementary Table 2.docx

Supplementary Table 2: Major oxide/element (wt.%) compositions of chromatite inclusions in clinopyroxene from PIC sample FW-20 using electron probe micro-analysis [a]

	SiO_2	TiO_2	Al_2O_3	Cr_2O_3	CrO_3	FeO	MgO	K_2O	Na_2O	CaO	ZnO	SO_2	SO_3	F	Cl	Total (Cr_2O_3, SO_2)[b]	Total (CrO_3, SO_3)[c]
Chromatite 1	0.23	0.03	0.07	44.61	58.97	0.18	2.10	1.46	0.18	26.04	0.04	3.65	4.63	2.73	0.23	81.55	96.89
Chromatite 2	0.17	0.00	0.05	41.16	54.40	0.15	0.63	1.12	0.16	27.42	0.05	5.12	6.49	2.65	0.23	78.93	93.54
Chromatite 3	0.32	0.04	0.06	36.77	48.59	0.17	0.56	0.26	0.37	33.52	0.00	5.92	7.49	3.07	0.04	81.11	94.50
Chromatite 4	0.30	0.01	0.04	35.53	46.95	0.17	1.36	0.24	0.72	32.59	0.00	6.28	7.94	2.71	0.16	80.13	93.21

[a] Electron probe micro-analysis run conditions: beam accelerating voltage = 15 kV; beam current = 35 nA; spotsize = 7 µm; counting times of 20 s on peak positions, and 10 s on two background positions located on either side of the peak position

[b] Raw elemental Cr and S wt.% values were converted to oxide wt.% for Cr_2O_3 and SO_2, which is the standard procedure for EPMA data reduction at the University of Melbourne

[c] Raw elemental Cr and S wt.% values were converted to oxide wt.% for CrO_3 and SO_3, before the total was recalculated using $CrO_3 + SO_3$ wt.% instead of $Cr_2O_3 + SO_2$ wt.%

Highlights

- First Tl isotope study of micas from metasomatised MARID and PIC mantle rocks
- All bar one sample has a mantle-like ε^{205}Tl value, contrasting with different genetic pathways laid out by previous studies
- PIC-kimberlite genetic link suggests mantle-like ε^{205}Tl values in kimberlites
- MARID parental melt derived by melting primitive mantle plus 1-30% mixed recycled component or 1-50% continental crust
- Possible kinetic isotope fractionation in one sample highlights need to integrate petrographic data in isotope studies